Cell

Nociceptor neurons direct goblet cells via a CGRP-RAMP1 axis to drive mucus production and gut barrier protection

Graphical abstract

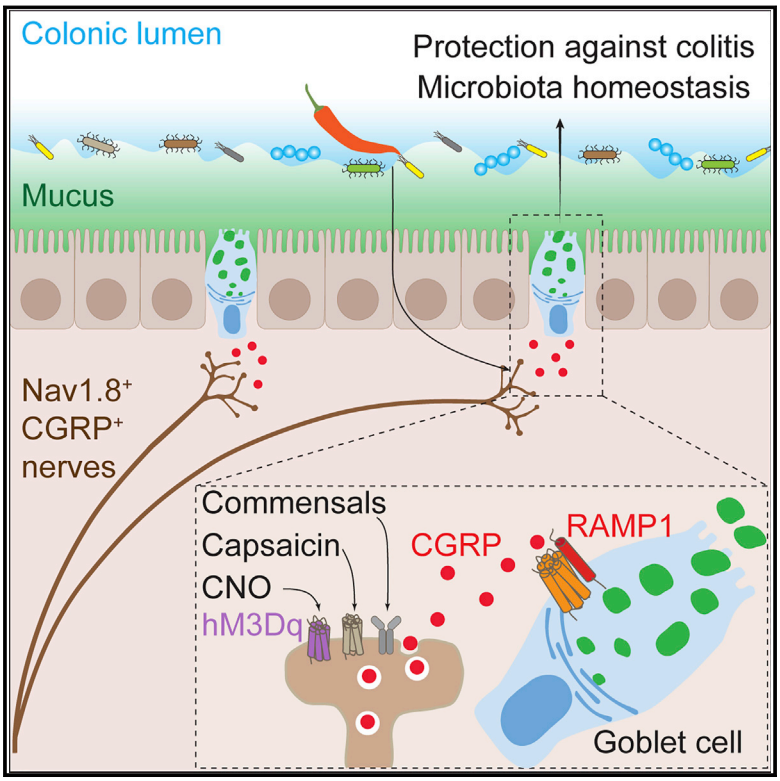

Authors

Daping Yang, Amanda Jacobson, Kimberly A. Meerschaert, ..., Jay R. Thiagarajah, Samantha J. Riesenfeld, Isaac M. Chiu

Correspondence

isaac_chiu@hms.harvard.edu

In brief

Pain sensory neurons induce mucus release from nearby intestinal goblet cells via a CGRP-Ramp1 axis in response to commensal and dietary cues to orchestrate gut mucosal protection.

Highlights

- Nav1.8^{+}CGRP^{+} nociceptors neighbor goblet cells and induce rapid mucus secretion
- Commensals trigger CGRP release, which signals to Ramp1 expressed by goblet cells
- Nociceptor or Ramp1 ablation leads to decreased mucus levels and microbial dysbiosis
- Neuron-goblet cell signaling via a CGRP-Ramp1 axis protects against colitis

Yang et al., 2022, Cell *185*, 1–16
October 27, 2022
https://doi.org/10.1016/j.cell.2022.09.024

CellPress

Please cite this article in press as: Yang et al., Nociceptor neurons direct goblet cells via a CGRP-RAMP1 axis to drive mucus production and gut barrier protection, Cell (2022), https://doi.org/10.1016/j.cell.2022.09.024

Cell

CellPress

Article

Nociceptor neurons direct goblet cells via a CGRP-RAMP1 axis to drive mucus production and gut barrier protection

Daping Yang,[1,12] Amanda Jacobson,[1,12] Kimberly A. Meerschaert,[1,13] Joseph Joy Sifakis,[2,13] Meng Wu,[1] Xi Chen,[3] Tiandi Yang,[1] Youlian Zhou,[1] Praju Vikas Anekal,[4] Rachel A. Rucker,[1] Deepika Sharma,[5] Alexandra Sontheimer-Phelps,[6] Glendon S. Wu,[1] Liwen Deng,[1] Michael D. Anderson,[3] Samantha Choi,[1] Dylan Neel,[1] Nicole Lee,[1] Dennis L. Kasper,[1] Bana Jabri,[5,7,8] Jun R. Huh,[1] Malin Johansson,[9] Jay R. Thiagarajah,[3] Samantha J. Riesenfeld,[5,7,10,11] and Isaac M. Chiu[1,14,*]

[1]Department of Immunology, Harvard Medical School, Boston, MA 02115, USA
[2]Department of Chemistry, University of Chicago, Chicago, IL 60637, USA
[3]Division of Gastroenterology, Hepatology and Nutrition, Boston Children's Hospital, Harvard Medical School, Boston, MA 02115, USA
[4]MicRoN Core, Harvard Medical School, Boston, MA 02115, USA
[5]Department of Medicine, University of Chicago, Chicago, IL 60637, USA
[6]Wyss Institute for Biologically Inspired Engineering, Harvard University, Boston, MA 02115, USA
[7]Committee on Immunology, University of Chicago, Chicago, IL 60637, USA
[8]Department of Pathology and Pediatrics, University of Chicago, Chicago, IL 60637, USA
[9]Department of Medical Biochemistry, Institute of Biomedicine, University of Gothenburg, Gothenburg 40530, Sweden
[10]Pritzker School of Molecular Engineering, University of Chicago, Chicago, IL 60637, USA
[11]Institute for Biophysical Dynamics, University of Chicago, Chicago, IL 60637, USA
[12]These authors contributed equally
[13]These authors contributed equally
[14]Lead contact
*Correspondence: isaac_chiu@hms.harvard.edu
https://doi.org/10.1016/j.cell.2022.09.024

SUMMARY

Neuroepithelial crosstalk is critical for gut physiology. However, the mechanisms by which sensory neurons communicate with epithelial cells to mediate gut barrier protection at homeostasis and during inflammation are not well understood. Here, we find that Nav1.8^{+}CGRP^{+} nociceptor neurons are juxtaposed with and signal to intestinal goblet cells to drive mucus secretion and gut protection. Nociceptor ablation led to decreased mucus thickness and dysbiosis, while chemogenetic nociceptor activation or capsaicin treatment induced mucus growth. Mouse and human goblet cells expressed Ramp1, receptor for the neuropeptide CGRP. Nociceptors signal via the CGRP-Ramp1 pathway to induce rapid goblet cell emptying and mucus secretion. Notably, commensal microbes activated nociceptors to control homeostatic CGRP release. In the absence of nociceptors or epithelial Ramp1, mice showed increased epithelial stress and susceptibility to colitis. Conversely, CGRP administration protected nociceptor-ablated mice against colitis. Our findings demonstrate a neuron-goblet cell axis that orchestrates gut mucosal barrier protection.

INTRODUCTION

Neuroepithelial crosstalk is fundamental for sensing and adapting to stimuli in the gastrointestinal (GI) tract (Furness et al., 2013; Kraus et al., 2021). Gut-innervating sensory neurons relay signals originating from epithelial cells to the brainstem and spinal cord through a gut-brain axis (Veiga-Fernandes and Mucida, 2016). Direct gut epithelial signaling to neurons has been described for enteroendocrine cells, which sense luminal signals and relay them to sensory nerves, resulting in metabolic adaptation or development of visceral pain (Bellono et al., 2017; Kaelberer et al., 2018; Ye et al., 2021). The molecular mechanisms underlying sensory neuron signaling to gut epithelial cells are less well understood.

The gut barrier is composed of epithelial cells connected by paracellular junctions and overlaid by a mucus layer, whose essential function is to prevent unregulated passage of luminal contents into underlying tissues (Chelakkot et al., 2018; Turner, 2009). Goblet cells are specialized epithelial cells that produce mucins and associated proteins to form the mucus layer, a loosening structural mucin gradient created by mucus-associated enzymes (Nyström et al., 2018). The mucus layer defends the tissue against microbial penetration while maintaining commensal homeostasis (Knoop and Newberry, 2018; Pelaseyed and

Please cite this article in press as: Yang et al., Nociceptor neurons direct goblet cells via a CGRP-RAMP1 axis to drive mucus production and gut barrier protection, Cell (2022), https://doi.org/10.1016/j.cell.2022.09.024

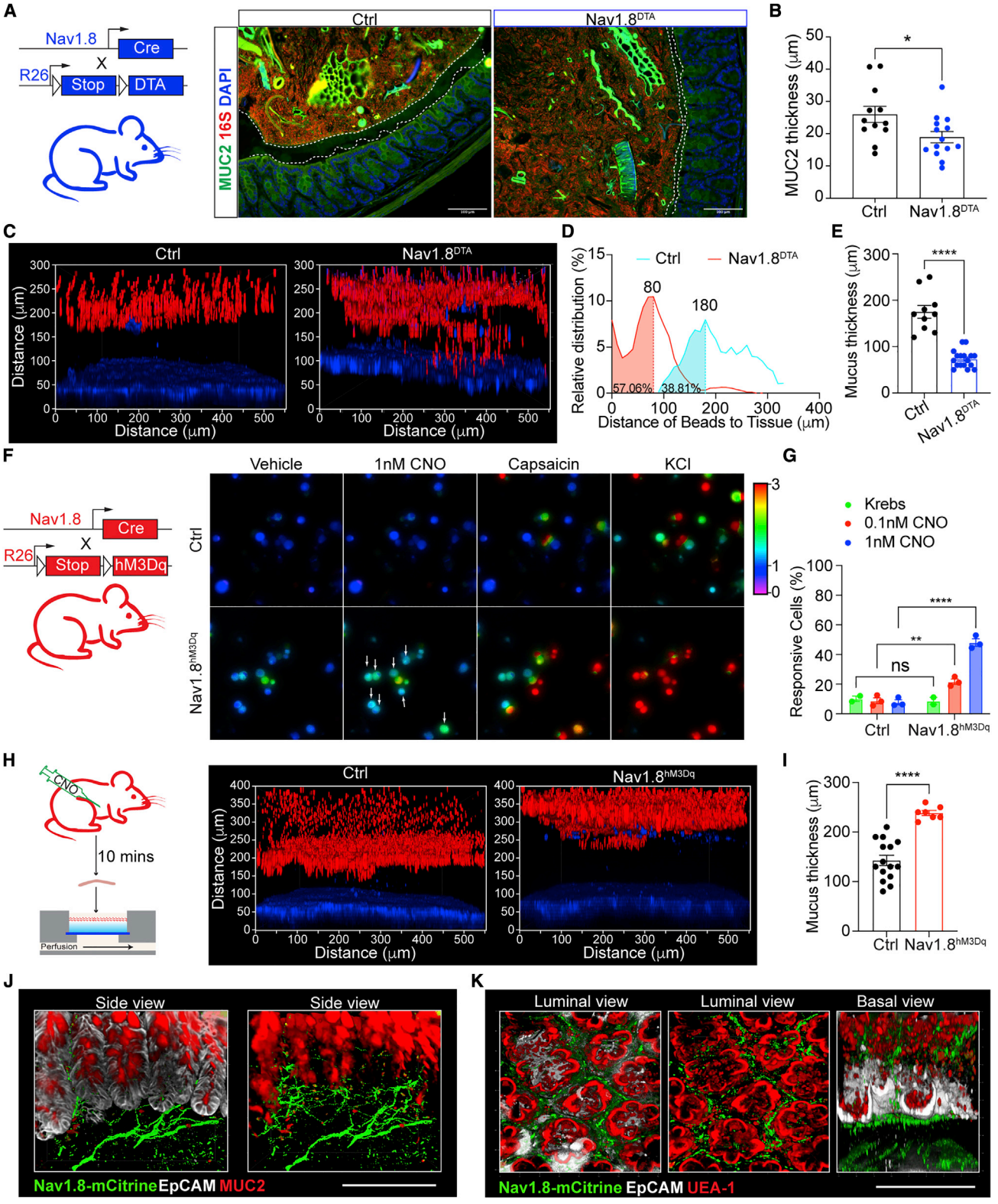

Figure 1. Nociceptors neighbor goblet cells and regulate colonic mucus production

(A) MUC2, 16S rDNA, and 4',6-diamidino-2-phenylindole (DAPI) staining in Nav1.8^{DTA} and control mouse colons.

(B) MUC2 thickness in Nav1.8^{DTA} and control colons (n = 12–14 mice/group).

(C) Colon explants showing epithelium (blue) overlaid with 1-μm beads (red) in Nav1.8^{DTA} and control mice.

(legend continued on next page)

Please cite this article in press as: Yang et al., Nociceptor neurons direct goblet cells via a CGRP-RAMP1 axis to drive mucus production and gut barrier protection, Cell (2022), https://doi.org/10.1016/j.cell.2022.09.024

Hansson, 2020). Mucus defects increase susceptibility to pathogens and are associated with development of inflammatory bowel diseases (Bergstrom et al., 2010; van der Post et al., 2019).

Microbial and immune cues are canonical triggers of mucus release from goblet cells (Birchenough et al., 2016; Wlodarska et al., 2014). The neurotransmitter acetylcholine (ACh) also induces mucus secretion from small intestine and colon explants (Halm and Halm, 1999; Specian and Neutra, 1980). Enteric neuron-derived IL-18 regulates goblet cell antimicrobial peptide production and host defense against *Salmonella* infection (Jarret et al., 2020). Few studies have evaluated the role of sensory neuroepithelial signaling in mucus secretion at homeostasis and during inflammation.

The GI tract is densely innervated by intrinsic enteric neurons and gut-extrinsic neurons, which cooperatively regulate diverse aspects of tissue physiology, including intestinal motility, nutrient absorption, sickness behavior, host defense, and pain (Veiga-Fernandes and Mucida, 2016; Yoo and Mazmanian, 2017). Nociceptors, characterized by expression of ion channels such as the voltage-gated sodium channel Nav1.8 and transient receptor potential vanilloid subtype 1 (TRPV1), are specialized sensory neurons that mediate pain, driving withdrawal and avoidance behaviors (Lagomarsino et al., 2021). Gut-innervating nociceptors are extrinsic sensory afferents arising from dorsal root ganglia (DRG), which, upon activation by noxious stimuli, transduce action potentials to the spinal cord to mediate visceral pain (Foster et al., 2017; Jacobson et al., 2021). At nociceptor peripheral nerve terminals, local release of neuropeptides, including calcitonin gene-related peptide (CGRP), can drive neurogenic inflammation through signaling to immune or vascular cells (Baral et al., 2019). The receptor for CGRP is formed by receptor activity modifying protein 1 (Ramp1) and its co-receptor, calcitonin receptor like receptor (Calcrl) (Moore and Salvatore, 2012). How nociceptors are involved in regulating the gut epithelial barrier at homeostasis and in inflammation is poorly defined.

Here, we demonstrate a critical role for nociceptor neurons and their signaling to goblet cells via a CGRP-Ramp1 axis in gut barrier protection. Nociceptor deficiency in mice led to decreased mucus thickness at homeostasis, while nociceptor activation induced mucus production. The CGRP co-receptors Ramp1 and Calcrl are expressed in goblet cells. In response to commensal and dietary cues, nociceptors released CGRP, which signaled through Ramp1 on goblet cells to induce mucus release. This nociceptor-goblet cell axis protected against colitis-induced immunopathology. Our findings demonstrate an intestinal neuroepithelial axis that orchestrates gut mucosal protection at homeostasis and during colitis pathogenesis.

RESULTS

Nociceptors are juxtaposed with goblet cells and mediate colonic mucus production

We bred *Nav1.8-Cre* mice with Cre-dependent *Rosa26-tdTomato* mice to label gut-innervating nociceptors. Nav1.8-tdTomato^{+} nerves were found in proximity to EpCAM^{+} epithelial cells in the colon (Figure S1A). We then bred *Nav1.8-Cre* mice with *Rosa26-DTA* mice to generate mice lacking Nav1.8^{+} nociceptors (Nav1.8^{DTA} mice) (Figure 1A) (Abrahamsen et al., 2008; Lai et al., 2020). Tyrosine hydroxylase (Th)$^{+}$ sympathetic nerves were intact in these mice (Figures S1B and S1C). Oral gavage of FITC-dextran in Nav1.8^{DTA} mice showed similar barrier permeability compared with control littermates (Figure S1D).

We next asked whether nociceptor ablation led to changes in the mucus layer. Mucin 2 (MUC2) immunostaining revealed that Nav1.8^{DTA} mice had thinner colon mucus layers compared with control mice (Figures 1A, 1B, and S1E). As mucus thickness can shrink due to fixation conditions, we next used a live colon explant assay overlaid with fluorescent beads to more accurately measure mucus thickness (Figure S1F) (Gustafsson et al., 2012). Bead distribution analysis showed that Nav1.8^{DTA} mice exhibited a thinner colonic mucus layer with higher bead penetrability compared with control littermates (Figures 1C–1E and S1G).

To investigate whether activating nociceptors is sufficient to promote mucus growth, we bred *Nav1.8-Cre* mice with hM3Dq reporter mice to drive expression of both mCitrine and hM3Dq, a Designer Receptor Exclusively Activated by Designer Drugs (DREADD) receptor whose ligand is clozapine N-oxide (CNO) (Nav1.8^{hM3Dq}) (Urban and Roth, 2015) (Figure 1F). CNO treatment induced dose-dependent calcium influx in cultured Nav1.8^{hM3Dq} DRG neurons but not control cells (Figures 1F, 1G, S1H, and S1I). CNO treatment of Nav1.8^{hM3Dq} mice rapidly increased mucus thickness compared with control mice (Figures 1H and 1I).

We observed Nav1.8-mCitrine^{+} nerves in close proximity to MUC2^{+}EpCAM^{+} goblet cells in colonic crypts (Figure 1J), suggesting they may interact. Nav1.8^{+} nerves were also juxtaposed with Ulex Europaeous Agglutinin -1 (UEA-1)$^{+}$EpCAM^{+} goblet cells in small intestine and colon (Figures 1K and S1J). We did not detect changes in overall MUC2^{+} goblet cell numbers between Nav1.8^{DTA} and control mice (Figures S1K–S1O). Hence, Nav1.8^{+} neurons are necessary and sufficient to regulate mucus production and may interact with goblet cells.

CGRP co-receptor Ramp1 is expressed in goblet cells and required for maintaining the mucus barrier

We hypothesized that nociceptors may directly signal to goblet cells via neuropeptides to facilitate mucus production. We

(D and E) Bead distribution (D) and mucus thickness (E) in Nav1.8^{DTA} and control colon explants (n = 3–5 areas/mouse and 3–4 mice/group); peak (mode) bead distance shown.
(F and G) Calcium influx in KCl-responsive DRG neurons from Nav1.8^{hM3Dq} and control mice induced by CNO (n = 3 per group).
(H and I) Colon explants (H) and mucus thickness (I) from Nav1.8^{hM3Dq} and control mice injected i.p. with CNO for 10 min. (n = 2–3 areas/mouse and 3–5 mice/group).
(J and K) Whole-mount colon tissues from Nav1.8^{hM3Dq} mice stained for mCitrine, EpCAM, MUC2, and UEA1. EpCAM removed in right (J) and middle (K). Scale bars, 100 μm. Student's t test in (B), (E), and (I). Two-way ANOVA in (G). Mean ± SEM. *p < 0.05, **p < 0.01, ***p < 0.001, and ****p < 0.0001.
See also Figure S1.

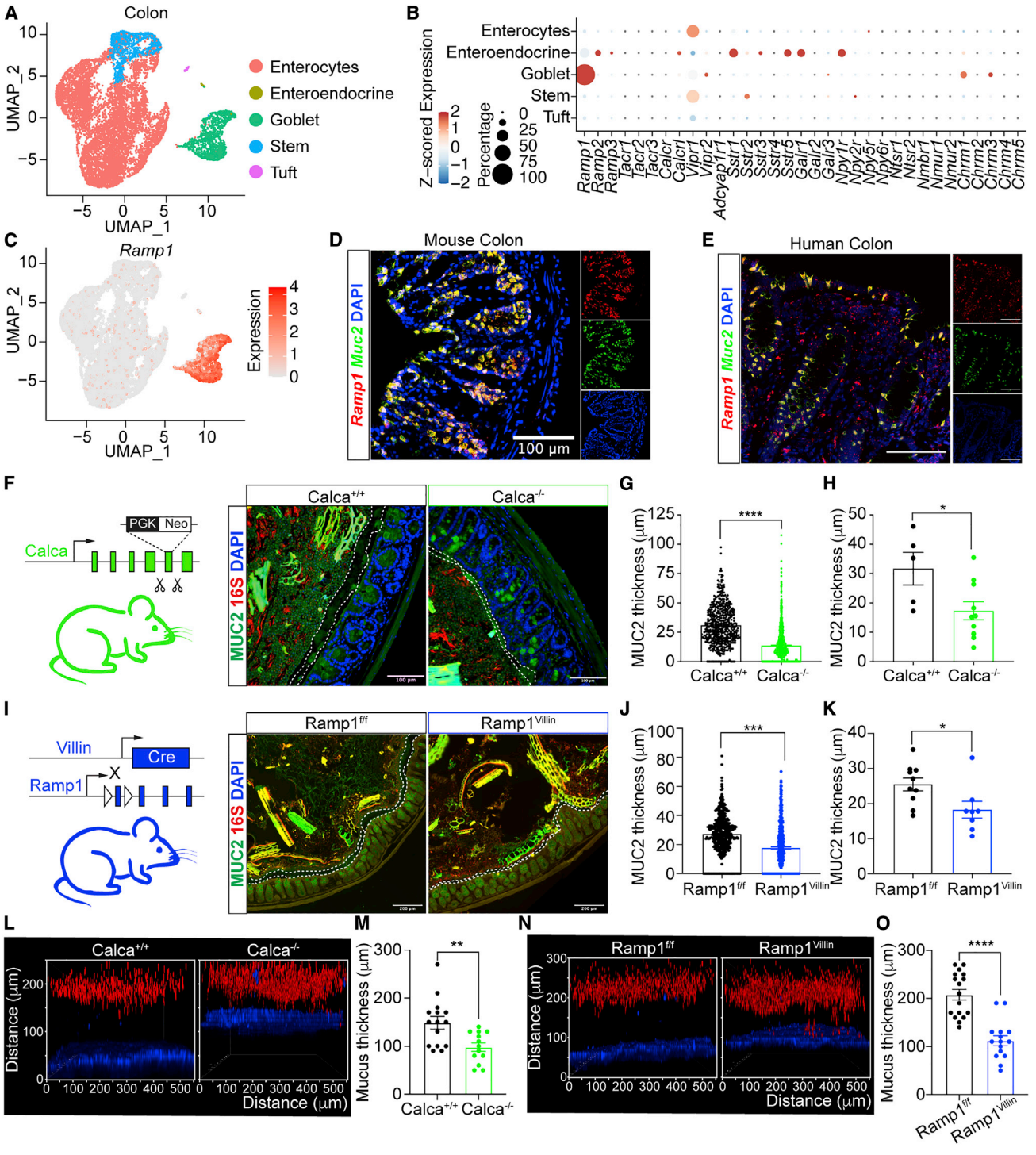

Figure 2. The CGRP co-receptor Ramp1 is expressed in goblet cells and maintains the mucus barrier

(A) UMAP of scRNA-seq data from colonic epithelial cells, colored by inferred cell type, from control *Nav1.8-Cre*$^{-}$*DTA*$^{fl/-}$ mice.

(B) Dot plot of average *Z*-scored expression of neuropeptide and neurotransmitter receptors in colonic epithelial cell subsets from (A).

(C) UMAP as in (A) showing *Ramp1* expression.

(D and E) *In situ* hybridization of *Ramp1* and *Muc2* in mouse colon (D) and *RAMP1* and *MUC2* in human colon (splenic flexure) (E).

(F–H) MUC2, 16S rDNA, and DAPI staining (F), MUC2 thickness per measurement (G), and per mouse (H) of colon tissue from *Calca*$^{+/+}$ and *Calca*$^{-/-}$ mice. (n = 5–10 mice/group).

(legend continued on next page)

performed single-cell RNA sequencing (scRNA-seq) of colonic and ileal EpCAM^{+}CD45^{-} epithelial cells from control (*Nav1.8-Cre*$^{-}$*DTA*$^{fl/-}$) mice. Five epithelial cell types, including goblet cells, were identified from coarse clusters based on expression of canonical marker genes (Figures 2A and S2A).

We surveyed colonic epithelial cells for expression of neuropeptide receptors (Figure 2B). Goblet cells uniquely expressed high levels of *Ramp1* and low levels of other neuropeptide receptors (Figures 2B and 2C). In the small intestine, expression of *Ramp1* was similarly high in goblet cells and absent in other epithelial cell types (Figures S2B and S2C), consistent with published scRNA-seq data of small intestine epithelial cells (Figure S2D) (Haber et al., 2017).

We also analyzed expression of Calcrl and the calcitonin receptor (Calcr), as both can form a complex with Ramp1 to bind CGRP (McLatchie et al., 1998; Salvatore et al., 2006). *Calcrl* was expressed in colonic goblet cells, but at lower levels compared with *Ramp1* (Figures 2B and S2E). By contrast, *Calcr* was not expressed (Figure S2E). As a comparison, we analyzed expression of muscarinic acetylcholine (ACh) receptors (mAChRs) (*Chrm1-5*), which play roles in mucus release (Gustafsson et al., 2021). We observed expression of *Chrm1* and *Chrm3* comparable to that of Calcrl (Figures 2B and S2E). A recent in-depth analysis of FACS-purified colonic MUC2^{+} goblet cells (Nyström et al., 2021) also revealed *Ramp1* and *Calcrl* expression (Figures S2F and S2G).

To spatially analyze expression in mouse and human gut tissues, we performed *in situ* hybridization. We observed colocalization of *Muc2* and *Ramp1* transcripts in goblet cells in the mouse colon (Figure 2D), mouse small intestine (Figure S2H), and colocalization of *MUC2* and *RAMP1* in human colon (Figures 2E and S2I). Immunostaining showed that Calcrl protein is expressed in UEA-1^{+} goblet cells and other epithelial cells in the mouse colon (Figure S2J). These data indicate that both components of the CGRP receptor, Ramp1 and Calcrl, are expressed in goblet cells.

We hypothesized that nociceptor-derived CGRP signals to Ramp1^{+} goblet cells to maintain mucus levels. CGRP has two isoforms: CGRPα and CGRPβ (Drokhlyansky et al., 2020; Russell et al., 2014). We found that CGRPα-deficient mice (*Calca*$^{-/-}$) showed significantly decreased mucus thickness compared with *Calca*$^{+/+}$ littermates (Figures 2F–2H). By contrast, CGRPβ-deficient mice (*Calcb*$^{-/-}$) did not show differences in goblet cell numbers or mucus thickness (Figures S2K and S2L).

We next asked whether epithelial Ramp1 signaling is required for colonic mucus maintenance. We bred Ramp1$^{fl/fl}$ mice with *Villin1-Cre* mice to specifically ablate Ramp1 in gut epithelial cells including goblet cells (Ramp1^{Villin} mice). While there was no difference in goblet cell numbers (Figure S2M), Ramp1^{Villin} mice had significantly thinner colonic mucus layers than control Ramp1$^{fl/fl}$ littermates (Figures 2I–2K). Decreased mucus thickness in *Calca*$^{-/-}$ and Ramp1^{Villin} mice compared with control littermates were confirmed in live colon explants (Figures 2L–2O). Therefore, CGRPα and epithelial expression of Ramp1 are required to maintain colonic mucus layers.

Nociceptors sense commensal microbes and dietary stimuli to release CGRP

Our data suggest that nociceptors communicate with goblet cells via CGRP to maintain the mucus barrier. Consistently, we observed CGRP colocalization with Nav1.8^{+} nerves in the colon (Figure S2N), and less CGRP in serum and colon explants from Nav1.8^{DTA} mice compared with control littermates (Figure 3A). Imaging of gut-innervating mesenteric nerves revealed ablation of CGRP^{+} nerves in Nav1.8^{DTA} mice, suggesting Nav1.8^{+} neurons as an important source of intestinal CGRP (Figure S2O).

Previous work showed that nociceptors can directly sense bacterial pathogens and their products (Baral et al., 2018; Chiu et al., 2013). We hypothesized that gut commensal microbes may trigger homeostatic nociceptor activation and CGRP release. We found significantly higher levels of CGRP in colon explants from specific-pathogen-free (SPF) mice compared with germ-free (GF) mice (Figure 3B). Fecal transplantation from SPF mice into GF mice significantly upregulated CGRP release in the colon (Figure 3C). Treatment of mice with the TRPV1 ligand resiniferatoxin (RTX) leads to chemical ablation of nociceptors, including those that innervate the gut (Lai et al., 2020). RTX pre-treatment blocked the upregulation of CGRP release in conventionalized GF mice (Figure 3C), suggesting a central role for nociceptors in microbiome-dependent CGRP release. Consistently, treatment of control mice with antibiotics decreased CGRP release (Figure 3D). However, antibiotics treatment did not reduce CGRP release in Nav1.8^{DTA} mice (Figure 3D), confirming the role of nociceptors as a CGRP source.

To determine whether commensal-derived products can directly activate nociceptors, we treated cultured DRG neurons with fecal supernatants. We found that fecal supernatant from SPF mice triggered significantly more DRG neuron activation, shown by calcium influx, and CGRP release, than that triggered by fecal supernatant from GF mice (Figures 3E–3J). Consistent with the increased CGRP release and previous studies (Johansson et al., 2015), the colonic mucus layer was significantly thicker in GF mice conventionalized with SPF feces compared with control GF mice (Figures 3K and 3L). Nociceptors were necessary for microbiome-dependent mucus layer growth, as pre-treatment of conventionalized mice with RTX resulted in a significantly thinner mucus layer (Figures 3K and 3L).

In addition to microbes, we hypothesized that dietary factors could trigger nociceptor activation and mucus production. Capsaicin, the active component of chili peppers, is a prototypic

(I–K) MUC2, 16S rDNA, and DAPI staining (I), MUC2 thickness per measurement (J) and per mouse (K) of colon tissue from Ramp1^{Villin} and Ramp1$^{fl/fl}$ mice. (n = 8–10 mice/group).

(L and M) Colonic explants (L) and mucus thickness (M) from *Calca*$^{+/+}$ and *Calca*$^{-/-}$ mice. (n = 3–5 area/mouse and 3–4 mice/group).

(N and O) Colonic explants (N) and mucus thickness (O) from Ramp1^{Villin} and Ramp1$^{fl/fl}$ mice. (n = 3–5 area/mouse and 3–4 mice/group).

Scale bars: 100 μm in (D–F) and (I). Mann-Whitney test in (G), (J), (M), and (O). Student's test in (H) and (K). Mean ± SEM. *p < 0.05, **p < 0.01, ***p < 0.001, and ****p < 0.0001.

See also Figure S2.

Please cite this article in press as: Yang et al., Nociceptor neurons direct goblet cells via a CGRP-RAMP1 axis to drive mucus production and gut barrier protection, Cell (2022), https://doi.org/10.1016/j.cell.2022.09.024

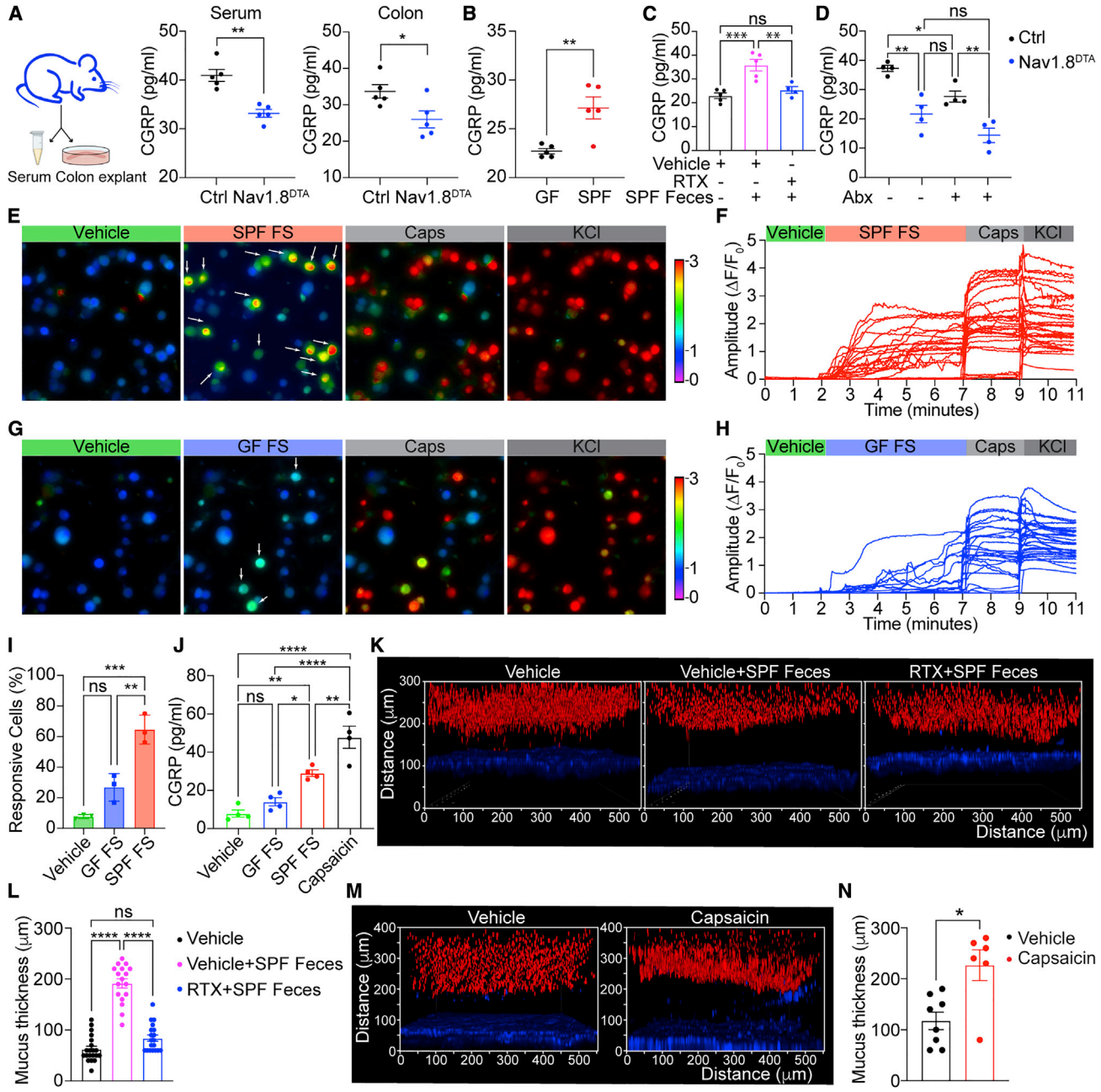

Figure 3. Nociceptors are activated by commensal cues and capsaicin to secrete CGRP

(A) Serum and colon CGRP levels in Nav1.8^{DTA} and control mice. (n = 5 mice/group).

(B) Colon CGRP levels in wild-type germ-free (GF) and specific-pathogen-free (SPF) mice. (n = 5 mice/group).

(C) Colon CGRP levels in vehicle-pretreated GF mice, vehicle- and resiniferatoxin (RTX)-pretreated GF mice transplanted with SPF feces. (n = 4–5 mice/group).

(D) Colon CGRP levels in Nav1.8^{DTA} and control mice treated with or without antibiotics (n = 4 mice/group).

(E–I) Calcium influx in KCl-responsive wild-type DRG neurons triggered by SPF fecal supernatant (SPF FS), GF fecal supernatant (GF FS), or capsaicin.

(J) CGRP levels produced by wild-type mouse DRG neurons stimulated with vehicle, GF FS, SPF FS, or capsaicin.

(K and L) Colonic explants (K) and mucus thickness (L) from mice in (C). (n = 3–5 area/mouse and 3–4 mice/group).

(M and N) Colonic explants (M) and mucus thickness (N) from wild-type B6 mice orally treated with vehicle or capsaicin (10 mg/kg) for 30 min. (n = 2 area/mouse and 3–4 mice/group).

Student's test in (A) and (B). One-way ANOVA in (C), (D), (I), and (J). Mann-Whitney test in (L) and (N). Mean ± SEM. ns, not significant. *p < 0.05, **p < 0.01, ***p < 0.001, and ****p < 0.0001.

Please cite this article in press as: Yang et al., Nociceptor neurons direct goblet cells via a CGRP-RAMP1 axis to drive mucus production and gut barrier protection, Cell (2022), https://doi.org/10.1016/j.cell.2022.09.024

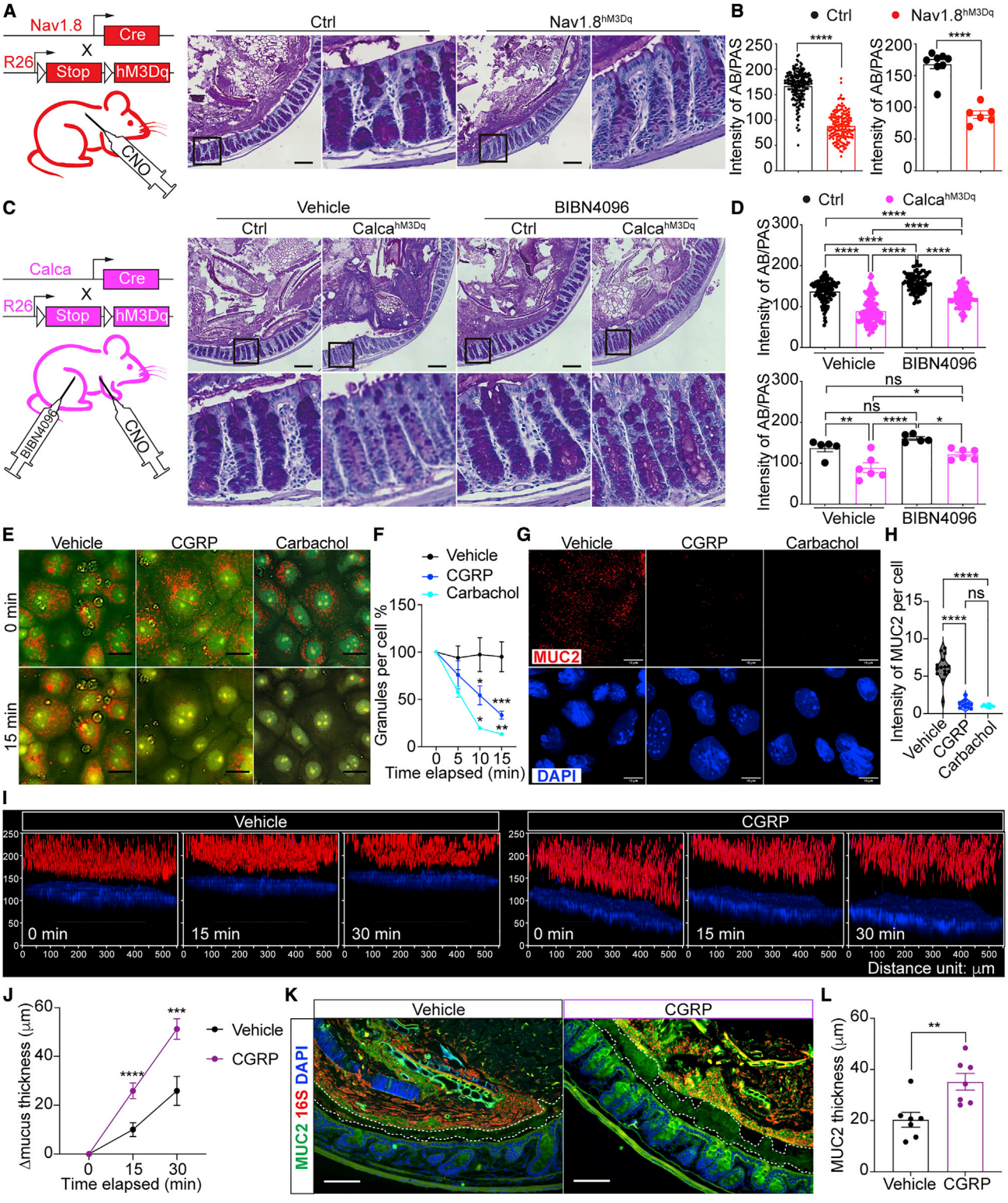

Figure 4. Nociceptor activation promotes goblet cell emptying and mucus secretion through CGRP-Ramp1 signaling

(A and B) AB/PAS (Alcian blue/periodic acid-Schiff) staining (A), intensity measurement (B) per crypt (left) and per mouse (right) of colon tissue from CNO-treated Nav1.8^{hM3Dq} and control mice. (n = 20–30 crypts/mouse and 6–8 mice/group).

(legend continued on next page)

TRPV1 ligand that activates nociceptors (Caterina et al., 1997). Capsaicin triggered robust DRG neuron activation and CGRP release *in vitro* (Figures 3E–3J). Oral gavage of capsaicin also dramatically induced increased colonic mucus thickness (Figures 3M and 3N). These results indicate that nociceptors can directly sense intestinal commensal cues and capsaicin to release CGRP.

Nociceptor activation induces goblet cell emptying and mucus growth through CGRP-Ramp1 signaling

We hypothesized that nociceptor activation is coupled to goblet cell emptying. We first confirmed that CNO induced CGRP release from Nav1.8^{hM3Dq} DRG neurons but not control neurons (Figure S3A). Next, we injected mice with CNO, observing rapid goblet cell emptying in Nav1.8^{hM3Dq} but not control mice as indicated by loss of periodic acid-Schiff (PAS)/Alcian blue (AB) staining (Figures 4A and 4B). We also generated Calca^{hM3Dq} mice to specifically activate CGRP^{+} neurons (Figure 4C). CNO treatment induced increased CGRP levels, as well as rapid goblet cell emptying in Calca^{hM3Dq} but not control mice (Figures 4C, 4D, and S3B). Pre-treatment of mice with the Ramp1 antagonist BIBN4096 significantly reduced goblet cell emptying upon CGRP^{+} neuron activation (Figures 4C and 4D), indicating that nociceptor neuron-dependent goblet cell mucus release relies on Ramp1 signaling. Consistent with goblet cell emptying, colonic mucus thickness in Calca^{hM3Dq} mice rapidly increased following CNO treatment compared with control mice (Figures S3C and S3D). As a control, activation of Th+ neurons in *Th-Cre*-induced hM3Dq DREADD (Th^{hM3Dq}) mice with CNO did not lead to goblet cell emptying (Figures S3E and S3F). These data indicate that nociceptor activation facilitates goblet cell emptying and mucus release through CGRP-Ramp1 signaling.

Our data point to nociceptor regulation of goblet cell function via CGRP, which is predicated on proximity between CGRP^{+} nerves and intestinal goblet cells. We observed close juxtaposition of CGRP-GFP^{+} nerves with MUC2^{+} goblet cells and UEA-1^{+} goblet cells in colonic crypts (Figures S3G and S3H), by imaging *Calca-GFP-DTR* mice that express eGFP under the *Calca* promoter (McCoy et al., 2013). These CGRP^{+} nerves were depleted by RTX-dependent nociceptor ablation (Figure S3I).

We next asked whether CGRP is sufficient to induce goblet cell emptying. We pre-loaded 2D-organoid-derived goblet cell cultures with Acridine orange, which fluoresces orange when accumulated in secretory cell vesicles (Shumilov et al., 2014). Treatment with CGRP or carbachol, a nonhydrolyzable mimic of ACh, resulted in rapid decrease of Acridine orange^{+} granules compared with treatment with vehicle, indicating goblet cell emptying (Figures 4E and 4F). Cells treated with CGRP or carbachol also exhibited significantly less intracellular MUC2 staining (Figures 4G and 4H). CGRP, but not vehicle treatment, induced a rapid increase of mucus thickness in live colon explants (Figures 4I, 4J, and S3J). Moreover, CGRP injection into wild-type (WT) mice led to a rapid and significant increase in colonic mucus thickness (Figures 4K, 4L, and S3K). Taken together, these data show that CGRP is sufficient to mediate goblet cell emptying, resulting in mucus layer growth.

We next determined whether CGRP induction of goblet cell emptying depends on Ramp1. CGRP i.p. injection induced goblet cell emptying in control Ramp1$^{fl/fl}$ mice but not in Ramp1^{Villin} mice (Figures S3L and S3M). Ramp1 has also been shown to be expressed on intestinal innate lymphoid cells (ILCs) (Nagashima et al., 2019; Wallrapp et al., 2019). However, ILC depletion had no effect on CGRP-induced goblet cell emptying (Figures S3N–S3P). Therefore, CGRP is sufficient to induce mucus secretion from goblet cells in a Ramp1-dependent but ILC-independent manner.

Loss of nociceptors induces microbial dysbiosis and gut epithelial transcriptional changes

The colonic mucus barrier is critical for maintenance of gut microbial homeostasis (Paone and Cani, 2020). We found that Nav1.8^{DTA} mice had a significantly different microbial composition in the colonic lumen and mucosa compared with control littermates, measured by weighted Unifrac β-diversity analysis (Figures 5A and S4A). Nav1.8^{DTA} lumen communities contained higher abundance of *Firmicutes* (*Bacillota*) families *Turibacteriaceae* and *Erysipelotrichaceae* compared with controls. Nav1.8^{DTA} mucosal communities displayed slightly lower levels of *Bacteroidetes* family S24-7 and *Firmicutes* family *Ruminococcaceae* compared with controls (Figure 5B). Among the most abundant genera, *Turicibacter* (of *Turicibacteriaceae* family) and *Allobaculum* (of *Erysipelotrichaceae* family) were expanded in Nav1.8^{DTA} luminal communities (Figure 5C), while Nav1.8^{DTA} mucosal communities exhibited lower abundance of S24-7 bacteria and *Oscillospira* sp. (of *Ruminococcaceae* family) (Figure 5D). *Turicibacter* and *Allobaculum* could regulate gut inflammation, with the former enhancing colitis pathogenesis in aged mice and the latter acting as a human intestinal mucus degrader (Liu et al., 2020; Shang et al., 2021; van Muijlwijk et al., 2021).

(C and D) AB/PAS staining (C) and intensity measurement (D) per crypt (upper) and per mouse (lower) of colon tissue from vehicle- or BIBN4096-pretreated Calca^{hM3Dq} and control mice after CNO injection (n = 20–30 crypts/mouse and 5–6 mice/group).

(E and F) Acridine orange (AO) staining (E) and normalized intensity measurement (F) of 2D organoid-derived wild-type primary goblet cell cultures treated with vehicle, CGRP, carbachol for the indicated time points. (n = 4–10 areas and 100–200 cells/area).

(G and H) MUC2 and DAPI staining (G) and intensity measurement (H) of primary wild-type goblet cell cultures treated with vehicle, CGRP, or carbachol for 15 min. (n = 8–15 areas and 100–200 cells/area).

(I and J) Wild-type mouse colonic explants (I) and mucus thickness growth (J) after vehicle or CGRP treatment for the indicated time points. (n = 3–5 areas/mouse and 4 mice/group).

(K and L) MUC2, 16S rDNA, and DAPI staining (K) and MUC2 thickness (L) of colon tissue from wild-type B6 mice 10 min after CGRP i.p. injection. (n = 7 mice/group).

Scale bars: 100 μm in (A), (C), and (K). Scale bars, 10 μm in (E) and (G). Mann-Whitney test in left (B) and top (D). Student's t test in right (B) and (L). Two-way ANOVA in bottom (D). One-way ANOVA in (H). Multiple t test in (F) and (J). Mean ± SEM. ns, not significant. *p < 0.05, **p < 0.01, ***p < 0.001, and ****p < 0.0001. See also Figure S3.

Please cite this article in press as: Yang et al., Nociceptor neurons direct goblet cells via a CGRP-RAMP1 axis to drive mucus production and gut barrier protection, Cell (2022), https://doi.org/10.1016/j.cell.2022.09.024

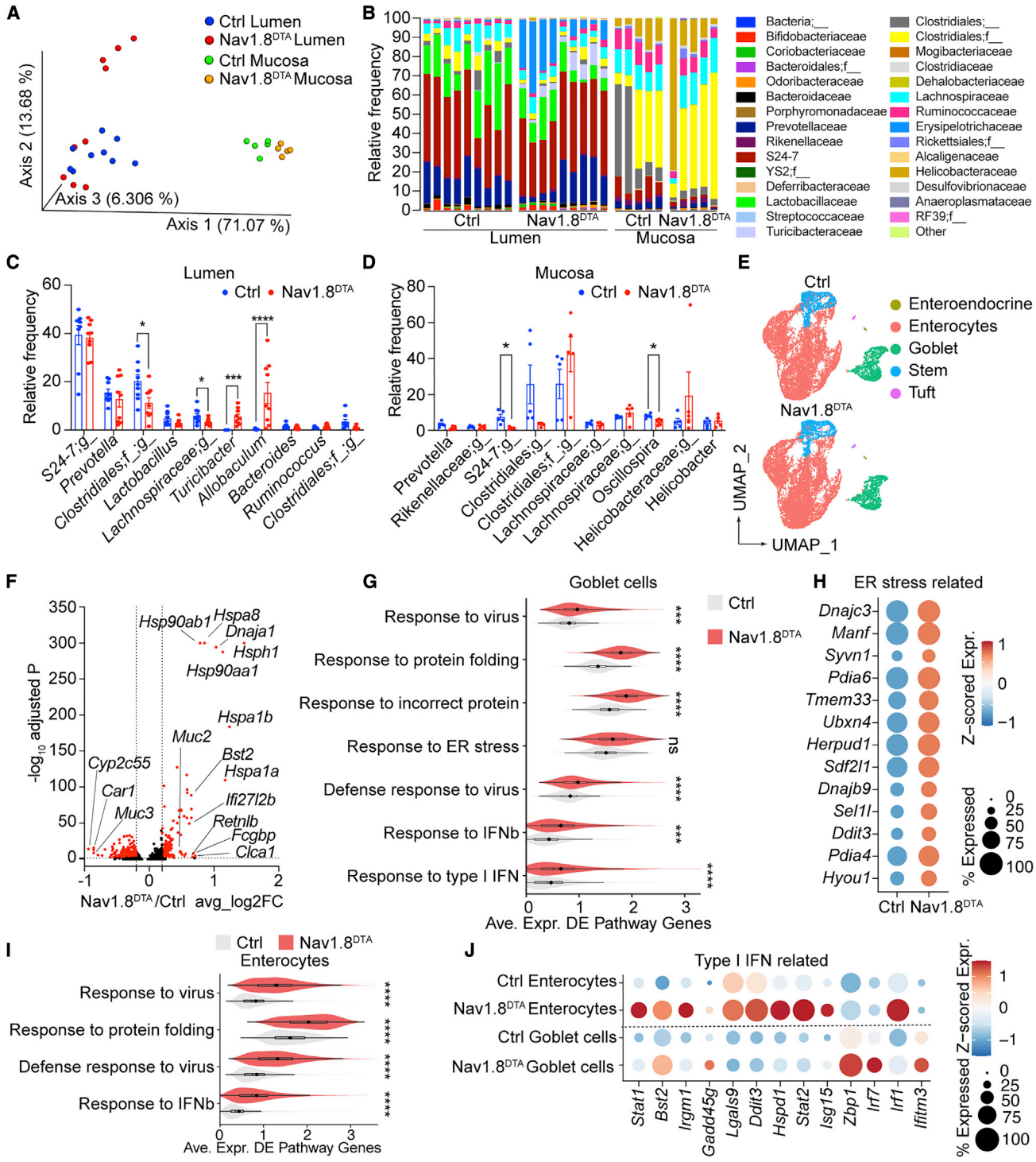

Figure 5. Nociceptor deficiency results in intestinal dysbiosis and epithelial stress

(A–D) Microbiome analysis: principal coordinates analysis (PCoA) of weighted UniFrac distance measurements (A), and family-level (B) and genus-level (C and D) analyses of the microbiome in colonic lumen contents (lumen) and mucosal scrapings (mucosa) of Nav1.8^{DTA} and control mice (n = 5–9 mice/group).

(E) UMAP of scRNA-seq profiles of colonic epithelial cells from control (top) and Nav1.8^{DTA} (bottom) mice.

(F) Volcano plot highlights 782 differentially expressed genes (DEGs; in red; $|\log_2$ fold change$|$ >0.2, adjusted $p < 0.05$) in Nav1.8^{DTA} versus control colonic goblet cells.

(G) Violin plots show distributions across colonic goblet cells in Nav1.8^{DTA} and control mice of the average expression of the DEGs, as in (F), that intersect with each of the indicated enriched pathways.

(legend continued on next page)

Please cite this article in press as: Yang et al., Nociceptor neurons direct goblet cells via a CGRP-RAMP1 axis to drive mucus production and gut barrier protection, Cell (2022), https://doi.org/10.1016/j.cell.2022.09.024

We hypothesized that loss of nociceptors could also lead to transcriptional changes in epithelial cells. We performed scRNA-seq analysis of ileal and colonic epithelial cells isolated from Nav1.8^{DTA} mice compared with control littermates. While we found no major changes in cell-type composition (Figures 5E and S4B), a comparison of colonic goblet cell transcriptional profiles from Nav1.8^{DTA} mice and controls identified 782 differentially expressed genes (DEGs) (Figure 5F). Gene set enrichment analysis using gene ontology (GO) indicated that goblet cells from Nav1.8^{DTA} mice had increased responses to protein folding, endoplasmic reticulum (ER) stress, and antiviral immunity (Figures 5G and 5H). We also observed significant transcriptional changes in enterocytes from Nav1.8^{DTA} mice, with increased responses to protein folding and antiviral immunity (Figure 5I). Goblet cells and enterocytes from Nav1.8^{DTA} mice showed increased expression of antiviral and type-I-IFN-induced genes (Figure 5J). We observed fewer transcriptional changes in ileal goblet cells (Figure S4C).

In contrast with decreased mucus thicknesses observed in Nav1.8^{DTA} mice, colonic goblet cells in these mice displayed slightly increased transcript levels for some mucus-related genes (Figure S4D), which was supported at the protein level by a subtle but significantly increased mucin staining intensity within goblet cells (Figures S4E and S4F). These results suggest that mucus layer defects in Nav1.8^{DTA} mice are not due to transcriptional downregulation.

We next asked whether nociceptor ablation affects mucus protein composition. We performed mass spectrometry of colon mucus collected from Nav1.8^{DTA} and littermate control mice. Analysis identified only 9 differentially expressed proteins between genotypes, mainly lipoproteins and extracellular matrix proteins (Figure S4G). MUC2 and MUC13, the two major mucin subtypes captured in the proteomics analysis, showed similar levels in Nav1.8^{DTA} and control mucus, consistent with transcript levels (Figures S4H and S4I). Western blot confirmed similar protein levels of MUC2 in Nav1.8^{DTA} and control mucus (Figure S4J). These data support a role for nociceptors in regulation of mucus thickness and goblet cell emptying, but not of mucus protein composition.

We also aimed to understand how Ramp1 signaling impacts gut epithelial cell transcription by performing scRNA-seq analysis of colonic epithelial cells isolated from Ramp1^{Villin} mice compared with controls. Loss of Ramp1 did not lead to overall changes in epithelial cell composition (Figures S4K and S4L). We identified 302 DEGs in colonic goblet cells (Figure S4M). GO enrichment analysis indicated that Ramp1^{Villin} goblet cells had an enhanced cellular response to ER stress and incorrect protein folding (Figures S4N and S5A), and enterocytes had an increased protein folding and antiviral responses (Figure S5B). We did not observe clear changes in mucus-related gene expression in Ramp1^{Villin} colonic goblet cells compared with controls (Figure S5C).

To highlight common aspects of the mouse models, we performed an intersectional analysis of both colonic scRNA-seq datasets and identified 108 common DEGs shared by Nav1.8^{DTA} and Ramp1^{Villin} goblet cells (Figure S5D), with a positive enrichment in genes related to heat shock and protein folding and a negative enrichment in genes related to cholesterol metabolism by GO analysis (Figures S5E and S4F). Enterocytes from both Nav1.8^{DTA} and Ramp1^{Villin} mice shared upregulation of cellular stress response pathways (Figures S5G and S5H). Taken together, our results indicate that nociceptors maintain gut microbiota composition at homeostasis and that loss of nociceptors or epithelial Ramp1 signaling leads to epithelial transcriptional changes that may reflect increased stress responses.

Nociceptors and CGRP-Ramp1 signaling regulate host protection against colitis

Despite loss of mucus, microbial dysbiosis, and epithelial changes in nociceptor-deficient mice, these mice displayed no changes at baseline in populations of lamina propria (LP) immune cells or intraepithelial lymphocytes (Figures S6A–S6G), nor changes in colon length or histology (Figures S6H–S6K). We hypothesized that these mice may be more susceptible to barrier damage. To test this, we treated Nav1.8^{DTA} and control mice with dextran sodium sulfate (DSS) to induce colitis. Pain is a major symptom of colitis. We measured visceromotor responses (VMR) induced by colorectal distension to detect visceral pain-like responses (Larauche et al., 2010). Control mice but not Nav1.8^{DTA} mice showed increased VMR after DSS treatment (Figure 6A).

Nav1.8^{DTA} mice displayed significantly more severe colitis compared with control mice, indicated by greater body weight loss, shorter colon length, worse colonic structure disruption, increased penetration of immune cells and goblet cell loss, and higher histology scores after DSS treatment (Figures 6B–6G and S6L). We also observed a significant increase in LP macrophages, monocytes, and neutrophils in Nav1.8^{DTA} mice (Figures 6H and S6M). Nav1.8^{DTA} mice and control mice consumed similar amounts of water throughout DSS treatment (Figure S6N). RTX-treated mice, which lack TRPV1^{+} nociceptors, also showed increased body weight loss, shorter colon lengths, and increased histology scores compared with control mice after DSS treatment (Figures 6I and S7A–S7D). These data indicate that nociceptors protect against pathology induced by DSS-induced colitis.

We observed increased colonic CGRP release after DSS treatment (Figure 6J). DSS treatment also induced colonic CGRP release in Nav1.8^{DTA} mice (Figure 6J), indicating that Nav1.8^{+} nociceptors are not the sole source of CGRP release during DSS colitis. Further analyses revealed a protective role for epithelial Ramp1 during colitis, as Ramp1^{Villin} mice displayed significantly greater body weight loss, shorter colon length, and increased histology scores (Figures 6K–6O and

(H) Dot plot of average *Z*-scored expression of ER-stress-related genes in colonic goblet cells from Nav1.8^{DTA} and control mice.
(I) Violin plot, analogous to (G), for DEGs in enterocytes from Nav1.8^{DTA} and control mice.
(J) Dot plot of average *Z*-scored expression of type I IFN-related genes in enterocytes and goblet cells from Nav1.8^{DTA} and control mice. Multiple t tests in (C and D). Mann-Whitney test in (G) and (I). ns, not significant. *$p < 0.05$, **$p < 0.01$, ***$p < 0.001$, and ****$p < 0.0001$.
See also Figures S4 and S5.

Please cite this article in press as: Yang et al., Nociceptor neurons direct goblet cells via a CGRP-RAMP1 axis to drive mucus production and gut barrier protection, Cell (2022), https://doi.org/10.1016/j.cell.2022.09.024

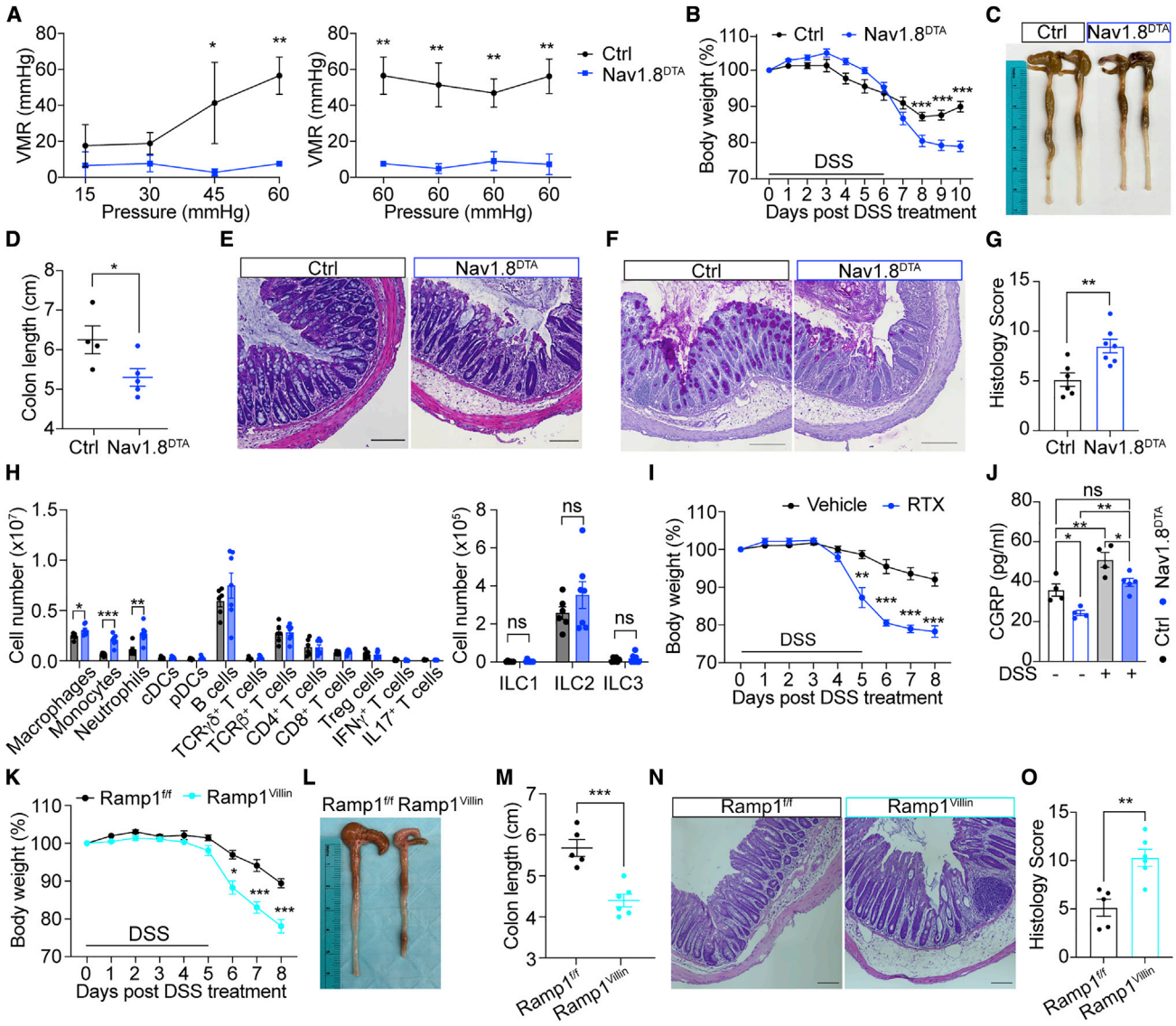

Figure 6. Nociceptors and epithelial Ramp1 are necessary for host protection against intestinal colitis

(A) Visceromotor responses (VMR) of Nav1.8^{DTA} and control mice 8 days post DSS treatment (n = 3 mice/group).

(B) Body weight of Nav1.8^{DTA} and control mice after DSS treatment (n = 9–10 mice/group).

(C–G) Representative colon image (C), colon length (D), H&E staining (E), AB/PAS staining (F), histology scoring per mouse (G) of mice in (B) on day 10 post DSS treatment. (n = 4 areas/mouse and 4–7 mice/group).

(H) Immune profiling of colonic lamina propria from mice in (B) on day 10 post DSS treatment (n = 6–7 mice/group).

(I) Body weight of RTX- and vehicle-pretreated mice post DSS treatment (n = 4 mice/group).

(J) Colon CGRP levels from Nav1.8^{DTA} and control mice treated with or without DSS for 5 days (n = 4 mice/group).

(K–O) Body weight (K), colon image (L), colon length (M), H&E staining (N), and histology scores per mouse (O) of Ramp1^{Villin} and Ramp1$^{fl/fl}$ mice 8 days post DSS treatment. (n = 4 areas/mouse and 5–6 mice/group).

Scale bars: 100 μm in (E), (F), and (N). Multiple t test in (A), (B), (H), (I), and (K). Student's test in (D), (G), (M), and (O). One-way ANOVA in (J). Mean ± SEM. ns, not significant. *p < 0.05, **p < 0.01, and ***p < 0.001.

See also Figure S7.

S7E–S7H). We observed a trend toward increased survival in Ramp1$^{fl/fl}$ mice compared with Ramp1^{Villin} mice at higher concentrations of DSS treatment (Figure S7F). Ramp1^{Villin} and littermate control mice exhibited similar colon lengths at baseline (Figures S7I and S7J).

To test the role of nociceptor activation during colitis, we treated Nav1.8^{hM3Dq} and control mice simultaneously with DSS and CNO. Of note, Nav1.8^{hM3Dq} mice drank less DSS-containing water during the first and fifth day of DSS treatment (Figure S7K), which is a caveat that limits our interpretation of these data (see

Please cite this article in press as: Yang et al., Nociceptor neurons direct goblet cells via a CGRP-RAMP1 axis to drive mucus production and gut barrier protection, Cell (2022), https://doi.org/10.1016/j.cell.2022.09.024

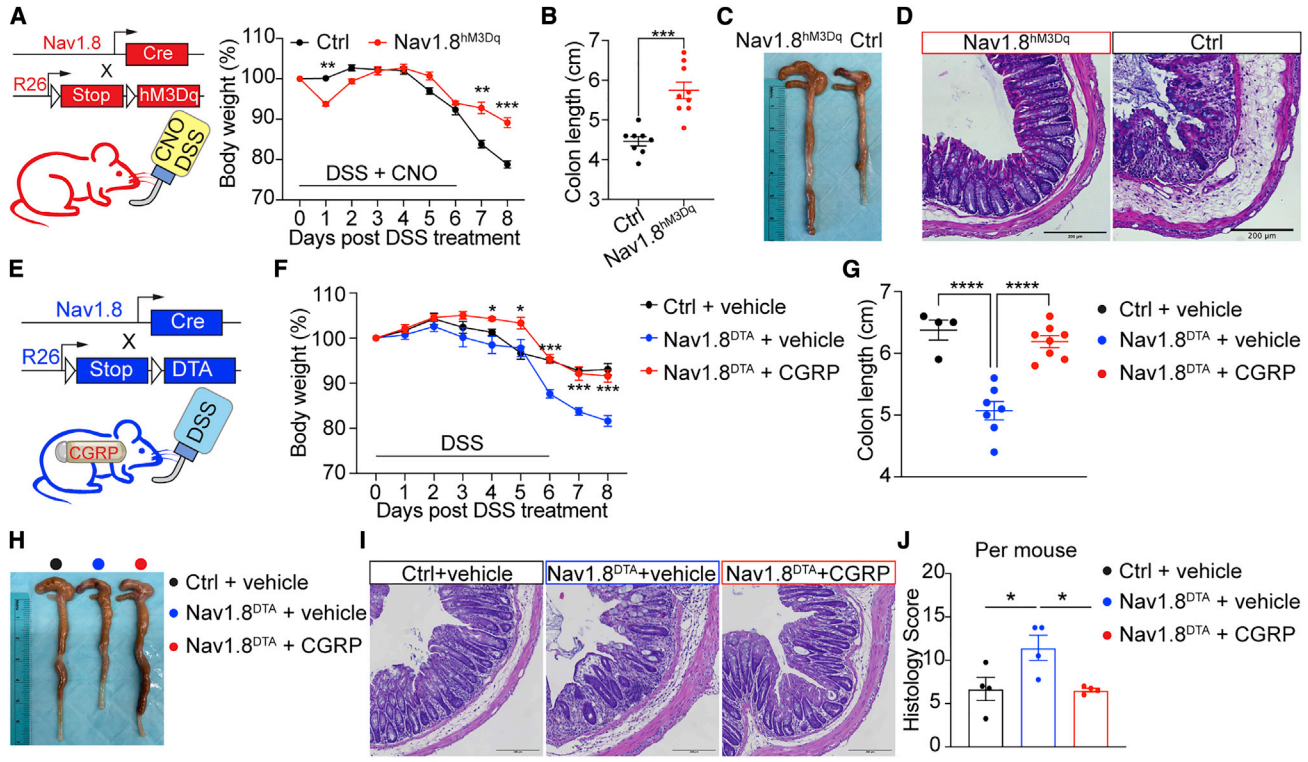

Figure 7. CGRP administration ameliorates intestinal colitis pathology

(A–D) Body weight (A), colon length (B), colon image (C), and H&E staining (D) of Nav1.8^{hM3Dq} and control mice 8 days post DSS plus CNO (0.5 μg/mL) treatment. (n = 8–9 mice/group).

(E) Nav1.8^{DTA} mice were s.c. implanted with osmotic pumps carrying either vehicle or CGRP. Control mice were s.c. implanted with osmotic pumps carrying vehicle. All mice were subjected to DSS treatment and sacrificed on day 8.

(F–J) Body weight (F), colon length (G), colon image (H), H&E staining (I), and histology scores per mouse (J) of mice in (E) (4 areas/mouse, n = 4 mice/group). Scale bars: 200 μm in (D) and (I). multiple t test in (A) and (F). Student's t test in (B). One-way ANOVA in (G) and (J). Mean ± SEM. ns, not significant. *p < 0.05, **p < 0.01, ***p < 0.001, and ****p < 0.0001.

See also Figure S7.

limitations of the study section). Nav1.8^{hM3Dq} mice displayed less body weight loss, longer colon lengths, and lower histology scores compared with control mice (Figures 7A–7D and S7L–S7M), indicating a milder colitis pathogenesis. Nociceptor activation also changed the microbiome of Nav1.8^{hM3Dq} mice compared with that of control mice after DSS and CNO treatment (Figures S7N–S7P). Taken together, these data demonstrate a critical role for nociceptors and the CGRP-Ramp1 signaling axis in regulating host protection against colitis.

CGRP administration rescues nociceptor-ablated mice from colitis

Given that Nav1.8^{DTA} mice have decreased intestinal CGRP and more severe colitis, we hypothesized that CGRP treatment could rescue the worsened pathogenesis present in Nav1.8^{DTA} mice. Nav1.8^{DTA} mice were subcutaneously implanted with an osmotic pump containing either CGRP or a vehicle control, facilitating continuous release of CGRP after transplantation. Following implantation, mice were treated with DSS (Figure 7E). While vehicle-treated Nav1.8^{DTA} mice exhibited worse immunopathology after DSS treatment compared with vehicle-treated control mice, CGRP-treated Nav1.8^{DTA} mice showed significantly less immunopathology from DSS pathogenesis, indicated by less body weight loss, longer colon lengths, and lower histology scores (Figures 7F–7J and S7Q–S7R). Collectively, these data suggest that CGRP treatment is sufficient to rescue Nav1.8^{DTA} mice from worsened intestinal colitis.

DISCUSSION

The canonical function of nociceptor neurons is to detect harmful stimuli, mediating pain perception and avoidance behaviors. In this study, we identify a role for nociceptors in driving intestinal mucus release through neuron-goblet cell communication. Nociceptor activation leads to release of CGRP, which acts on Ramp1 on intestinal goblet cells to induce rapid mucus secretion. Nociceptors and Ramp1 are required to maintain the mucus layer and microbiome composition at homeostasis. In addition, the nociceptor-CGRP-Ramp1 signaling axis provides protection during intestinal colitis. Therefore, we highlight a critical role of nociceptor-goblet cell communication in gut barrier protection.

Please cite this article in press as: Yang et al., Nociceptor neurons direct goblet cells via a CGRP-RAMP1 axis to drive mucus production and gut barrier protection, Cell (2022), https://doi.org/10.1016/j.cell.2022.09.024

Mucin exocytosis is thought to rely on calcium signaling, and cAMP signaling mediates fluid secretion that accompanies mucus granule release (Lee and Foskett, 2014; Yang et al., 2013). CGRP-Ramp1 signaling is known to induce both cAMP increases and calcium influx in neurons (Hosokawa et al., 2010; Russell et al., 2014). The specific signaling pathways within goblet cells required for CGRP-dependent emptying remain to be fully determined.

The CGRP-Ramp1 goblet cell signaling axis described in our study may have relevance for other mucosal tissues including the respiratory tract. Nociceptor nerves are juxtaposed with lung epithelial cells, and optogenetic stimulation of vagal sensory neurons induces increased mucin transcription and release (Talbot et al., 2020b).

While neuroimmune circuitry is well described in the gut (Cardoso et al., 2021; Gabanyi et al., 2016; Godinho-Silva et al., 2019; Muller et al., 2020; Seillet et al., 2020; Talbot et al., 2020a; Xu et al., 2019), less is known about how neurons and epithelial cells communicate. We previously found that gut-extrinsic nociceptors suppressed microfold (M) cells in small intestine Peyer's Patches and maintained levels of segmented filamentous bacteria (SFB), thereby limiting *Salmonella* invasion (Lai et al., 2020). Given that SFB does not colonize the mouse colon (Farkas et al., 2015; Lai et al., 2020), nor are M cells present at baseline in the GI tract (Kimura et al., 2015), we do not expect changes in these factors to affect goblet cell mucus release described in this study. However, it is possible that mucus defects could be upstream of and contribute to the changes observed in our previous study.

Our study adds to the far-reaching role of CGRP in mucosal biology. CGRP regulates macrophages, neutrophils, and group 2 innate lymphoid cells (ILC2s) (Baral et al., 2019; Nagashima et al., 2019; Wallrapp et al., 2019). Our work reveals the broad impact of this neuropeptide on epithelial cells. While our study focuses on CGRP from sensory neurons, enteric neurons and ILC2s have also been shown to produce CGRP (Wallrapp et al., 2019; Xu et al., 2019). Questions remain as to whether these other cells can signal via CGRP to goblet cells.

Calcium influx is sufficient to induce CGRP release from nociceptors, whereas production of pain perception requires high threshold stimulation and action potential transduction to the central nervous system (CNS). We posit that at homeostasis gut microbe-derived factors stimulate nociceptors at a low level, leading to homoeostatic CGRP release but not pain perception. However, in situations of barrier breach such as during colitis, increased stimuli further enhance nociceptor activation, leading to pain perception. Nociception coupled with mucus production may be a way for the gut to accelerate the removal of harmful substances.

Pain is a major symptom of inflammatory bowel diseases (Bielefeldt et al., 2009). However, acute pain and its accompanying release of CGRP may protect the gut barrier. We confirmed that eliminating nociceptors in DSS-induced colitis leads to worsening of pathology (Kawashima-Takeda et al., 2017; Utsumi et al., 2018), consistent with another study showing that CGRP and TRPV1 play a protective role during colitis (Engel et al., 2011). Given that pain treatments are often used to treat patients with colitis, it may be important to consider detrimental consequences of blocking pain. Anti-CGRP therapies are widely used to treat or prevent chronic migraine (Cohen et al., 2021). While these therapies are currently lauded as having minimal side effects (Vandervorst et al., 2021), our work reveals potential detrimental side effects on the gut barrier. Indeed, recent clinical studies show that anti-CGRP migraine therapeutics caused constipation in patients (Holzer and Holzer-Petsche, 2021). Overall, our findings demonstrate a nociceptor neuron-goblet cell axis that critically orchestrates gut barrier maintenance at homeostasis and protection during intestinal inflammation.

Limitations of the study

While our study indicates that nociceptors mediate mucus production and gut barrier protection, we cannot rule out CGRP-independent mechanisms as Nav1.8^{+} neurons express other neuropeptides (VIP, substance P) and mediators that could act on goblet cells. The Ramp1 antagonist BIBN4096 did not completely prevent CGRP-dependent goblet cell emptying. Therefore, CGRP may indirectly regulate mucus production via impacting non-goblet epithelial, immune, or stromal cells that signal to goblet cells. Alternatively, nociceptor activation could regulate other branches of the nervous system (e.g., ChAT+ enteric or parasympathetic neurons), which release mediators (e.g., ACh) that impact goblet cell emptying. A limitation in our DSS colitis studies of Nav1.8^{hM3Dq} mice was that we observed a difference in water consumption during DSS treatment such that Nav1.8^{hM3Dq} mice consumed less water than controls. This limits the conclusions drawn, as activation of pain pathways in Nav1.8^{hM3Dq} mice could have limited DSS intake through avoidance and contributed to the milder disease severity. Future approaches are needed to dissociate pain-induced avoidance behaviors from neuronal activation and epithelial changes.

STAR★METHODS

Detailed methods are provided in the online version of this paper and include the following:

- KEY RESOURCES TABLE
- RESOURCE AVAILABILITY
  - Lead contact
  - Materials availability
  - Data and code availability
- EXPERIMENTAL MODEL AND SUBJECT DETAILS
  - Mice
  - Human intestinal tissue samples
- METHOD DETAILS
  - DRG isolation and culture
  - CGRP release of DRG neuron cultures, colonic explants, and serum
  - 3D colonoid and 2D primary epithelial cell culture
  - Immunostaining of mucin
  - Immunostaining of goblet cells
  - H&E and AB/PAS staining analysis
  - RNAscope
  - *Ex vivo* mucus analysis
  - Whole mount immunostaining
  - Intestinal epithelial cell and immune cell isolation

- Flow cytometry
- ILC depletion
- 10X scRNA-seq of colon
- inDrops scRNA-seq of ileum
- TRPV1 nociceptor neuron ablation
- DSS-induced colitis
- Gut permeability assay
- Osmotic pump implantation
- Visceromotor response (VMR) assay
- 16S rDNA sequencing and data analysis
- Western blot of MUC2

● QUANTIFICATION AND STATISTICAL ANALYSIS

- Single-cell RNA-seq data analysis
- Mass spectrometry-based mucus proteomics
- 16S rDNA sequencing data analysis
- Analysis of published single-cell data

SUPPLEMENTAL INFORMATION

Supplemental information can be found online at https://doi.org/10.1016/j.cell.2022.09.024.

ACKNOWLEDGMENTS

We thank Himanish Basu, Felipe Pinho-Ribeiro, Antonia Wallrapp, Nicole Almanzar, Chambit Paik, Alos Diallo, Eunha Kim, Valentina Lagomarsino, Paula Montero Llopis, Beatriz Martinez Abad (U. Gothenburg), Nicole Lai (Kallyope), and Muriel Larauche (UCLA) for technical help. We thank Gunnar Hansson (U. Gothenburg), Chuan Wu (NIH), Ruaidhri Jackson (Harvard Medical School), and Wayne Lencer (Boston Children's Hospital) for helpful discussions. We thank Meenakshi Rao (Boston Children's Hospital) for *Calcb*$^{-/-}$ mice. We thank HDDC Microscopy and Histopathology Core (NIDDK P30DK034854) and BIDMC Histology Core for histology; MicRoN Core at HMS for imaging analysis; Bauer Core, HMS Single-Cell Core, and Harvard Chan Bioinformatics Core for scRNA-seq. This work was supported by National Institutes of Health (NIH) R01DK127257, Food Allergy Science Initiative, Kenneth Rainin Foundation to I.M.C.; NIH T32 in pediatric gastroenterology (T32 DK007447) to A.J.; R35GM142683 (NIGMS) to J.R.T. and P30DK034854 (J.R.T. and M.D.A.); Digestive Diseases Research Core Center P30 DK42086 at University of Chicago to B.J.

AUTHOR CONTRIBUTIONS

Planning and conceptualization, D.Y., A.J., and I.M.C.; mucus analysis, D.Y., A.J., and P.V.A.; confocal imaging, D.Y. and A.J.; histological analysis, D.Y., A.J., R.A.R., and G.S.W.; computational analysis, J.J.S., S.J.R., and D.N.; calcium imaging, D.Y. and K.A.M.; microbiome analysis, D.Y., M.W., and N.L.; colorectal distension, Y.Z.; flow cytometry, ELISAs, D.Y., L.D., and S.C.; cell and explant analysis, D.Y., A.J., A.S.-P., D.S., and M.D.A.; organoid cultures, X.C.; mass spectrometry, T.Y.; key resources, D.L.K., B.J., J.R.H., J.R.T., and M.J.; writing – original draft, D.Y., A.J., and I.M.C.; editing manuscript, D.Y., A.J., S.J.R., and I.M.C.

DECLARATION OF INTERESTS

A.J. is an employee of Genentech, Inc. I.M.C. serves on scientific advisory boards of GSK Pharmaceuticals and Limm Therapeutics. His lab receives research support from Moderna Inc. and AbbVie/Allergan Pharmaceuticals.

INCLUSION AND DIVERSITY

We worked to ensure sex balance in the selection of non-human subjects. One or more of the authors of this paper self-identifies as a gender minority in their field of research.

Received: March 2, 2022
Revised: July 22, 2022
Accepted: September 14, 2022
Published: October 14, 2022

REFERENCES

Abrahamsen, B., Zhao, J., Asante, C.O., Cendan, C.M., Marsh, S., Martinez-Barbera, J.P., Nassar, M.A., Dickenson, A.H., and Wood, J.N. (2008). The cell and molecular basis of mechanical, cold, and inflammatory pain. Science *321*, 702–705.

Baral, P., Udit, S., and Chiu, I.M. (2019). Pain and immunity: implications for host defence. Nat. Rev. Immunol. *19*, 433–447.

Baral, P., Umans, B.D., Li, L., Wallrapp, A., Bist, M., Kirschbaum, T., Wei, Y., Zhou, Y., Kuchroo, V.K., Burkett, P.R., et al. (2018). Nociceptor sensory neurons suppress neutrophil and γδ T cell responses in bacterial lung infections and lethal pneumonia. Nat. Med. *24*, 417–426.

Bellono, N.W., Bayrer, J.R., Leitch, D.B., Castro, J., Zhang, C., O'Donnell, T.A., Brierley, S.M., Ingraham, H.A., and Julius, D. (2017). Enterochromaffin cells are gut chemosensors that couple to sensory neural pathways. Cell *170*, 185–198.e16.

Bergstrom, K.S., Kissoon-Singh, V., Gibson, D.L., Ma, C., Montero, M., Sham, H.P., Ryz, N., Huang, T., Velcich, A., Finlay, B.B., et al. (2010). Muc2 protects against lethal infectious colitis by disassociating pathogenic and commensal bacteria from the colonic mucosa. PLOS Pathog. *6*, e1000902.

Bielefeldt, K., Davis, B., and Binion, D.G. (2009). Pain and inflammatory bowel disease. Inflamm. Bowel Dis. *15*, 778–788.

Birchenough, G.M., Nyström, E.E., Johansson, M.E., and Hansson, G.C. (2016). A sentinel goblet cell guards the colonic crypt by triggering Nlrp6-dependent Muc2 secretion. Science *352*, 1535–1542.

Cardoso, F., Klein Wolterink, R.G.J., Godinho-Silva, C., Domingues, R.G., Ribeiro, H., da Silva, J.A., Mahú, I., Domingos, A.I., and Veiga-Fernandes, H. (2021). Neuro-mesenchymal units control ILC2 and obesity via a brain-adipose circuit. Nature *597*, 410–414.

Caterina, M.J., Schumacher, M.A., Tominaga, M., Rosen, T.A., Levine, J.D., and Julius, D. (1997). The capsaicin receptor: a heat-activated ion channel in the pain pathway. Nature *389*, 816–824.

Chelakkot, C., Ghim, J., and Ryu, S.H. (2018). Mechanisms regulating intestinal barrier integrity and its pathological implications. Exp. Mol. Med. *50*, 1–9.

Chiu, I.M., Heesters, B.A., Ghasemlou, N., Von Hehn, C.A., Zhao, F., Tran, J., Wainger, B., Strominger, A., Muralidharan, S., Horswill, A.R., et al. (2013). Bacteria activate sensory neurons that modulate pain and inflammation. Nature *501*, 52–57.

Cohen, J.M., Ning, X., Kessler, Y., Rasamoelisolo, M., Campos, V.R., Seminerio, M.J., Krasenbaum, L.J., Shen, H., and Stratton, J. (2021). Immunogenicity of biologic therapies for migraine: a review of current evidence. J. Headache Pain *22*, 3.

Cox, J., Hein, M.Y., Luber, C.A., Paron, I., Nagaraj, N., and Mann, M. (2014). Accurate proteome-wide label-free quantification by delayed normalization and maximal peptide ratio extraction, termed MaxLFQ. Mol. Cell. Proteomics *13*, 2513–2526.

Cox, J., Neuhauser, N., Michalski, A., Scheltema, R.A., Olsen, J.V., and Mann, M. (2011). Andromeda: a peptide search engine integrated into the MaxQuant environment. J. Proteome Res. *10*, 1794–1805.

Drokhlyansky, E., Smillie, C.S., Van Wittenberghe, N., Ericsson, M., Griffin, G.K., Eraslan, G., Dionne, D., Cuoco, M.S., Goder-Reiser, M.N., Sharova, T., et al. (2020). The human and mouse enteric nervous system at single-cell resolution. Cell *182*, 1606–1622.e23.

Engel, M.A., Leffler, A., Niedermirtl, F., Babes, A., Zimmermann, K., Filipović, M.R., Izydorczyk, I., Eberhardt, M., Kichko, T.I., Mueller-Tribbensee, S.M., et al. (2011). TRPA1 and substance P mediate colitis in mice. Gastroenterology *141*, 1346–1358.

Farkas, A.M., Panea, C., Goto, Y., Nakato, G., Galan-Diez, M., Narushima, S., Honda, K., and Ivanov, I.I. (2015). Induction of Th17 cells by segmented filamentous bacteria in the murine intestine. J. Immunol. Methods *421*, 104–111.

Foster, S.L., Seehus, C.R., Woolf, C.J., and Talbot, S. (2017). Sense and immunity: context-dependent neuro-immune interplay. Front. Immunol. *8*, 1463.

Furness, J.B., Rivera, L.R., Cho, H.J., Bravo, D.M., and Callaghan, B. (2013). The gut as a sensory organ. Nat. Rev. Gastroenterol. Hepatol. *10*, 729–740.

Gabanyi, I., Muller, P.A., Feighery, L., Oliveira, T.Y., Costa-Pinto, F.A., and Mucida, D. (2016). Neuro-immune interactions drive tissue programming in intestinal macrophages. Cell *164*, 378–391.

Godinho-Silva, C., Cardoso, F., and Veiga-Fernandes, H. (2019). Neuro-immune cell units: A new paradigm in physiology. Annu. Rev. Immunol. *37*, 19–46.

Gustafsson, J.K., Davis, J.E., Rappai, T., McDonald, K.G., Kulkarni, D.H., Knoop, K.A., Hogan, S.P., Fitzpatrick, J.A., Lencer, W.I., and Newberry, R.D. (2021). Intestinal goblet cells sample and deliver lumenal antigens by regulated endocytic uptake and transcytosis. eLife *10*, e67292.

Gustafsson, J.K., Ermund, A., Johansson, M.E., Schütte, A., Hansson, G.C., and Sjövall, H. (2012). An ex vivo method for studying mucus formation, properties, and thickness in human colonic biopsies and mouse small and large intestinal explants. Am. J. Physiol. Gastrointest. Liver Physiol. *302*, G430–G438.

Haber, A.L., Biton, M., Rogel, N., Herbst, R.H., Shekhar, K., Smillie, C., Burgin, G., Delorey, T.M., Howitt, M.R., Katz, Y., et al. (2017). A single-cell survey of the small intestinal epithelium. Nature *551*, 333–339.

Hafemeister, C., and Satija, R. (2019). Normalization and variance stabilization of single-cell RNA-seq data using regularized negative binomial regression. Genome Biol. *20*, 296.

Halm, D.R., and Halm, S.T. (1999). Secretagogue response of goblet cells and columnar cells in human colonic crypts. Am. J. Physiol. *277*, C501–C522.

Hao, Y., Hao, S., Andersen-Nissen, E., Mauck, W.M., 3rd, Zheng, S., Butler, A., Lee, M.J., Wilk, A.J., Darby, C., Zager, M., et al. (2021). Integrated analysis of multimodal single-cell data. Cell *184*, 3573–3587.e29.

Holzer, P., and Holzer-Petsche, U. (2021). Constipation caused by anti-calcitonin gene-related peptide migraine therapeutics explained by antagonism of calcitonin gene-related peptide's motor-stimulating and prosecretory function in the intestine. Front. Physiol. *12*, 820006.

Hosokawa, S., Endoh, T., Shibukawa, Y., Tsumura, M., Ichikawa, H., Tazaki, M., and Furusawa, M. (2010). Calcitonin gene-related peptide- and adrenomedullin-induced facilitation of calcium current by different signal pathways in nucleus tractus solitarius. Brain Res. *1327*, 47–55.

Jacobson, A., Yang, D., Vella, M., and Chiu, I.M. (2021). The intestinal neuro-immune axis: crosstalk between neurons, immune cells, and microbes. Mucosal Immunol. *14*, 555–565.

Jarret, A., Jackson, R., Duizer, C., Healy, M.E., Zhao, J., Rone, J.M., Bielecki, P., Sefik, E., Roulis, M., Rice, T., et al. (2020). Enteric nervous system-derived IL-18 orchestrates mucosal barrier immunity. Cell *180*, 50–63.e12.

Johansson, M.E., and Hansson, G.C. (2012). Preservation of mucus in histological sections, immunostaining of mucins in fixed tissue, and localization of bacteria with FISH. Methods Mol. Biol. *842*, 229–235.

Johansson, M.E., Jakobsson, H.E., Holmén-Larsson, J., Schütte, A., Ermund, A., Rodríguez-Piñeiro, A.M., Arike, L., Wising, C., Svensson, F., Bäckhed, F., and Hansson, G.C. (2015). Normalization of host intestinal mucus layers requires long-term microbial colonization. Cell Host Microbe *18*, 582–592.

Kaelberer, M.M., Buchanan, K.L., Klein, M.E., Barth, B.B., Montoya, M.M., Shen, X., and Bohórquez, D.V. (2018). A gut-brain neural circuit for nutrient sensory transduction. Science *361*, eaat5236.

Kawashima-Takeda, N., Ito, Y., Nishizawa, N., Kawashima, R., Tanaka, K., Tsujikawa, K., Watanabe, M., and Majima, M. (2017). RAMP1 suppresses mucosal injury from dextran sodium sulfate-induced colitis in mice. J. Gastroenterol. Hepatol. *32*, 809–818.

Kimura, S., Yamakami-Kimura, M., Obata, Y., Hase, K., Kitamura, H., Ohno, H., and Iwanaga, T. (2015). Visualization of the entire differentiation process of murine M cells: suppression of their maturation in cecal patches. Mucosal Immunol. *8*, 650–660.

Klein, A.M., Mazutis, L., Akartuna, I., Tallapragada, N., Veres, A., Li, V., Peshkin, L., Weitz, D.A., and Kirschner, M.W. (2015). Droplet barcoding for single-cell transcriptomics applied to embryonic stem cells. Cell *161*, 1187–1201.

Knoop, K.A., and Newberry, R.D. (2018). Goblet cells: multifaceted players in immunity at mucosal surfaces. Mucosal Immunol. *11*, 1551–1557.

Koelink, P.J., Wildenberg, M.E., Stitt, L.W., Feagan, B.G., Koldijk, M., van 't Wout, A.B., Atreya, R., Vieth, M., Brandse, J.F., Duijst, S., et al. (2018). Development of Reliable, Valid and Responsive Scoring Systems for Endoscopy and Histology in Animal Models for Inflammatory Bowel Disease. J Crohns Colitis *12*, 794–803.

Kraus, A., Buckley, K.M., and Salinas, I. (2021). Sensing the world and its dangers: an evolutionary perspective in neuroimmunology. eLife *10*, e66706.

Kuczynski, J., Stombaugh, J., Walters, W.A., Gonzalez, A., Caporaso, J.G., and Knight, R. (2012). Using QIIME to analyze 16S rRNA gene sequences from microbial communities. Curr. Protoc. Bioinform. *36*, 10.7.1–10.7.20. https://doi.org/10.1002/0471250953.bi1007s36.

Lagomarsino, V.N., Kostic, A.D., and Chiu, I.M. (2021). Mechanisms of microbial-neuronal interactions in pain and nociception. Neurobiol. Pain *9*, 100056.

Lai, N.Y., Musser, M.A., Pinho-Ribeiro, F.A., Baral, P., Jacobson, A., Ma, P., Potts, D.E., Chen, Z., Paik, D., Soualhi, S., et al. (2020). Gut-innervating nociceptor neurons regulate Peyer's patch microfold cells and SFB levels to mediate salmonella host defense. Cell *180*, 33–49.e22.

Larauche, M., Gourcerol, G., Million, M., Adelson, D.W., and Taché, Y. (2010). Repeated psychological stress-induced alterations of visceral sensitivity and colonic motor functions in mice: influence of surgery and postoperative single housing on visceromotor responses. Stress *13*, 343–354.

Lee, R.J., and Foskett, J.K. (2014). Ca^{2+} signaling and fluid secretion by secretory cells of the airway epithelium. Cell Calcium *55*, 325–336.

Liu, A., Lv, H., Wang, H., Yang, H., Li, Y., and Qian, J. (2020). Aging increases the severity of colitis and the related changes to the gut barrier and gut microbiota in humans and mice. J. Gerontol. A Biol. Sci. Med. Sci. *75*, 1284–1292.

McCoy, E.S., Taylor-Blake, B., Street, S.E., Pribisko, A.L., Zheng, J., and Zylka, M.J. (2013). Peptidergic CGRPalpha primary sensory neurons encode heat and itch and tonically suppress sensitivity to cold. Neuron *78*, 138–151.

McLatchie, L.M., Fraser, N.J., Main, M.J., Wise, A., Brown, J., Thompson, N., Solari, R., Lee, M.G., and Foord, S.M. (1998). RAMPs regulate the transport and ligand specificity of the calcitonin-receptor-like receptor. Nature *393*, 333–339.

Moore, E.L., and Salvatore, C.A. (2012). Targeting a family B GPCR/RAMP receptor complex: CGRP receptor antagonists and migraine. Br. J. Pharmacol. *166*, 66–78.

Muller, P.A., Schneeberger, M., Matheis, F., Wang, P., Kerner, Z., Ilanges, A., Pellegrino, K., Del Marmol, J., Castro, T.B.R., Furuichi, M., et al. (2020). Microbiota modulate sympathetic neurons via a gut-brain circuit. Nature *585*, 441–446.

Nagashima, H., Mahlakõiv, T., Shih, H.Y., Davis, F.P., Meylan, F., Huang, Y., Harrison, O.J., Yao, C., Mikami, Y., Urban, J.F., Jr., et al. (2019). Neuropeptide CGRP limits Group 2 innate lymphoid cell responses and constrains Type 2 inflammation. Immunity *51*, 682–695.e6.

Nalle, S.C., Zuo, L., Ong, M.L.D.M., Singh, G., Worthylake, A.M., Choi, W., Manresa, M.C., Southworth, A.P., Edelblum, K.L., Baker, G.J., et al. (2019). Graft-versus-host disease propagation depends on increased intestinal epithelial tight junction permeability. J. Clin. Invest. *129*, 902–914.

Nyström, E.E.L., Birchenough, G.M.H., van der Post, S., Arike, L., Gruber, A.D., Hansson, G.C., and Johansson, M.E.V. (2018). Calcium-activated chloride channel Regulator 1 (CLCA1) controls mucus expansion in colon by proteolytic activity. EBiomedicine *33*, 134–143.

Nyström, E.E.L., Martinez-Abad, B., Arike, L., Birchenough, G.M.H., Nonnecke, E.B., Castillo, P.A., Svensson, F., Bevins, C.L., Hansson, G.C., and Johansson, M.E.V. (2021). An intercrypt subpopulation of goblet cells is essential for colonic mucus barrier function. Science *372*, eabb1590.

Oh-Hashi, Y., Shindo, T., Kurihara, Y., Imai, T., Wang, Y., Morita, H., Imai, Y., Kayaba, Y., Nishimatsu, H., Suematsu, Y., et al. (2001). Elevated sympathetic nervous activity in mice deficient in alphaCGRP. Circ. Res. *89*, 983–990.

Paone, P., and Cani, P.D. (2020). Mucus barrier, mucins and gut microbiota: the expected slimy partners? Gut *69*, 2232–2243.

Pelaseyed, T., and Hansson, G.C. (2020). Membrane mucins of the intestine at a glance. J. Cell Sci. *133*, jcs240929.

Picelli, S., Faridani, O.R., Björklund, A.K., Winberg, G., Sagasser, S., and Sandberg, R. (2014). Full-length RNA-seq from single cells using Smart-seq2. Nat. Protoc. *9*, 171–181.

Pinho-Ribeiro, F.A., Baddal, B., Haarsma, R., O'Seaghdha, M., Yang, N.J., Blake, K.J., Portley, M., Verri, W.A., Dale, J.B., Wessels, M.R., and Chiu, I.M. (2018). Blocking neuronal signaling to immune cells treats streptococcal invasive infection. Cell *173*, 1083–1097.e22.

Russell, F.A., King, R., Smillie, S.J., Kodji, X., and Brain, S.D. (2014). Calcitonin gene-related peptide: physiology and pathophysiology. Physiol. Rev. *94*, 1099–1142.

Salvatore, C.A., Mallee, J.J., Bell, I.M., Zartman, C.B., Williams, T.M., Koblan, K.S., and Kane, S.A. (2006). Identification and pharmacological characterization of domains involved in binding of CGRP receptor antagonists to the calcitonin-like receptor. Biochemistry *45*, 1881–1887.

Sato, T., Stange, D.E., Ferrante, M., Vries, R.G., Van Es, J.H., Van den Brink, S., Van Houdt, W.J., Pronk, A., Van Gorp, J., Siersema, P.D., and Clevers, H. (2011). Long-term expansion of epithelial organoids from human colon, adenoma, adenocarcinoma, and Barrett's epithelium. Gastroenterology *141*, 1762–1772.

Seillet, C., Luong, K., Tellier, J., Jacquelot, N., Shen, R.D., Hickey, P., Wimmer, V.C., Whitehead, L., Rogers, K., Smyth, G.K., et al. (2020). The neuropeptide VIP confers anticipatory mucosal immunity by regulating ILC3 activity. Nat. Immunol. *21*, 168–177.

Shang, L., Liu, H., Yu, H., Chen, M., Yang, T., Zeng, X., and Qiao, S. (2021). Core altered microorganisms in colitis mouse model: A comprehensive time-point and fecal microbiota transplantation analysis. Antibiotics, *10* (Basel), p. 643.

Shevchenko, A., Tomas, H., Havlis, J., Olsen, J.V., and Mann, M. (2006). In-gel digestion for mass spectrometric characterization of proteins and proteomes. Nat. Protoc. *1*, 2856–2860.

Shumilov, D., Popov, A., Fudala, R., Akopova, I., Gryczynski, I., Borejdo, J., Gryczynski, Z., and Grygorczyk, R. (2014). Real-time imaging of exocytotic mucin release and swelling in Calu-3 cells using acridine orange. Methods *66*, 312–324.

Sonnenberg, G.F., Monticelli, L.A., Alenghat, T., Fung, T.C., Hutnick, N.A., Kunisawa, J., Shibata, N., Grunberg, S., Sinha, R., Zahm, A.M., et al. (2012). Innate lymphoid cells promote anatomical containment of lymphoid-resident commensal bacteria. Science *336*, 1321–1325.

Specian, R.D., and Neutra, M.R. (1980). Mechanism of rapid mucus secretion in goblet cells stimulated by acetylcholine. J. Cell Biol. *85*, 626–640.

Talbot, J., Hahn, P., Kroehling, L., Nguyen, H., Li, D., and Littman, D.R. (2020a). Feeding-dependent VIP neuron-ILC3 circuit regulates the intestinal barrier. Nature *579*, 575–580.

Talbot, S., Doyle, B., Huang, J., Wang, J.C., Ahmadi, M., Roberson, D.P., Yekkirala, A., Foster, S.L., Browne, L.E., Bean, B.P., et al. (2020b). Vagal sensory neurons drive mucous cell metaplasia. J. Allergy Clin. Immunol. *145*, 1693–1696.e4.

Thompson, B.J., Washington, M.K., Kurre, U., Singh, M., Rula, E.Y., and Emeson, R.B. (2008). Protective roles of alpha-calcitonin and beta-calcitonin gene-related peptide in spontaneous and experimentally induced colitis. Dig. Dis. Sci. *53*, 229–241.

Turner, J.R. (2009). Intestinal mucosal barrier function in health and disease. Nat. Rev. Immunol. *9*, 799–809.

Tyanova, S., Albrechtsen, R., Kronqvist, P., Cox, J., Mann, M., and Geiger, T. (2016). Proteomic maps of breast cancer subtypes. Nat. Commun. *7*, 10259.

Urban, D.J., and Roth, B.L. (2015). DREADDs (designer receptors exclusively activated by designer drugs): chemogenetic tools with therapeutic utility. Annu. Rev. Pharmacol. Toxicol. *55*, 399–417.

Utsumi, D., Matsumoto, K., Tsukahara, T., Amagase, K., Tominaga, M., and Kato, S. (2018). Transient receptor potential vanilloid 1 and transient receptor potential ankyrin 1 contribute to the progression of colonic inflammation in dextran sulfate sodium-induced colitis in mice: links to calcitonin gene-related peptide and substance P. J. Pharmacol. Sci. *136*, 121–132.

van der Post, S., Jabbar, K.S., Birchenough, G., Arike, L., Akhtar, N., Sjovall, H., Johansson, M.E.V., and Hansson, G.C. (2019). Structural weakening of the colonic mucus barrier is an early event in ulcerative colitis pathogenesis. Gut *68*, 2142–2151.

van Muijlwijk, G.H., van Mierlo, G., Jansen, P.W.T.C., Vermeulen, M., Bleumink-Pluym, N.M.C., Palm, N.W., van Putten, J.P.M., and de Zoete, M.R. (2021). Identification of Allobaculum mucolyticum as a novel human intestinal mucin degrader. Gut Microbes *13*, 1966278.

Vandervorst, F., Van Deun, L., Van Dycke, A., Paemeleire, K., Reuter, U., Schoenen, J., and Versijpt, J. (2021). CGRP monoclonal antibodies in migraine: an efficacy and tolerability comparison with standard prophylactic drugs. J. Headache Pain *22*, 128.

Veiga-Fernandes, H., and Mucida, D. (2016). Neuro-immune interactions at barrier surfaces. Cell *165*, 801–811.

Wallrapp, A., Burkett, P.R., Riesenfeld, S.J., Kim, S.J., Christian, E., Abdulnour, R.-E.E., Thakore, P.I., Schnell, A., Lambden, C., Herbst, R.H., et al. (2019). Calcitonin gene-related peptide negatively regulates alarmin-driven Type 2 innate lymphoid cell responses. Immunity *51*, 709–723.e6.

Wlodarska, M., Thaiss, C.A., Nowarski, R., Henao-Mejia, J., Zhang, J.P., Brown, E.M., Frankel, G., Levy, M., Katz, M.N., Philbrick, W.M., et al. (2014). NLRP6 inflammasome orchestrates the colonic host-microbial interface by regulating goblet cell mucus secretion. Cell *156*, 1045–1059.

Xu, H., Ding, J., Porter, C.B.M., Wallrapp, A., Tabaka, M., Ma, S., Fu, S., Guo, X., Riesenfeld, S.J., Su, C., et al. (2019). Transcriptional atlas of intestinal immune cells reveals that neuropeptide alpha-CGRP modulates Group 2 innate lymphoid cell responses. Immunity *51*, 696–708.e9.

Yang, N., Garcia, M.A., and Quinton, P.M. (2013). Normal mucus formation requires cAMP-dependent HCO3- secretion and Ca2+-mediated mucin exocytosis. J. Physiol. *591*, 4581–4593.

Ye, L., Bae, M., Cassilly, C.D., Jabba, S.V., Thorpe, D.W., Martin, A.M., Lu, H.Y., Wang, J., Thompson, J.D., Lickwar, C.R., et al. (2021). Enteroendocrine cells sense bacterial tryptophan catabolites to activate enteric and vagal neuronal pathways. Cell Host Microbe *29*, 179–196.e9.

Yoo, B.B., and Mazmanian, S.K. (2017). The enteric network: interactions between the immune and nervous systems of the gut. Immunity *46*, 910–926.

Yu, G., Wang, L.G., Han, Y., and He, Q.Y. (2012). clusterProfiler: an R package for comparing biological themes among gene clusters. Omics *16*, 284–287.

Zilionis, R., Nainys, J., Veres, A., Savova, V., Zemmour, D., Klein, A.M., and Mazutis, L. (2017). Single-cell barcoding and sequencing using droplet microfluidics. Nat. Protoc. *12*, 44–73.

Please cite this article in press as: Yang et al., Nociceptor neurons direct goblet cells via a CGRP-RAMP1 axis to drive mucus production and gut barrier protection, Cell (2022), https://doi.org/10.1016/j.cell.2022.09.024

STAR★METHODS

KEY RESOURCES TABLE

REAGENT or RESOURCE	SOURCE	IDENTIFIER
Antibodies		
Rabbit anti-Muc2 polyclonal antibody	Santa Cruz Biotechnology	No longer available RRID: AB_2146667
Rabbit anti-Muc2 polyclonal antibody	Genetex	Cat# GTX100664 RRID: AB_1950958
Rabbit anti-CALCRL polyclonal antibody	Thermo fisher	Cat# PA5-50644 RRID: AB_2636097
Rat anti-mouse CD90.2 (30H12)	Bio X Cell	Cat# BP0066 RRID: AB_1107682
Rat anti-EpCAM Monoclonal antibody	eBioscience	Cat# 17-5791-82 RRID: AB_2716944
Rabbit anti-Calcitonin Gene Related Peptide (CGRP) polyclonal antibody	ImmunoStar	Cat# 24112 RRID: AB_572217
Goat anti-mCherry polyclonal antibody	OriGene Technologies	Cat# AB0040-200 RRID: AB_2333093
Chicken anti-GFP polyclonal antibody	Novus Biologicals	Cat# NB100-1614 RRID: AB_10001164
Rabbit anti-Tyrosine Hydroxylase Antibody	EMD Millipore	Cat# AB152 RRID: AB_390204
Donkey anti-rabbit DyLight 488	Abcam	Cat# ab98488 RRID: AB_10676096
Donkey anti-rabbit Alexa 594	Abcam	Cat# ab150076 RRID: AB_2782993
Goat anti-chicken Alexa 488	Abcam	Cat# ab150173 RRID: AB_2827653
Donkey anti-rat Alexa 647	Abcam	Cat# ab150155 RRID: AB_2813835
Mouse anti-CD45 Pacific Blue	BioLegend	Cat# 103126 RRID: AB_493535
Mouse anti-TCR-b chain PE/Cy7	BioLegend	Cat# 109221 RRID: AB_893627
Mouse anti-TCR gamma/delta Brilliant Violet 605	BioLegend	Cat# 118129 RRID: AB_2563356
Mouse anti-mouse CD4 Brilliant Violet 650	BioLegend	Cat# 100469 RRID: AB_2783035
Mouse anti-mouse CD8a PerCP/Cy5.5	BioLegend	Cat# 100733 RRID: AB_2075239
Mouse anti-FOXP3 Alexa Fluor 488	BioLegend	Cat# 126405 RRID: AB_1089114
Mouse anti-IL17A PE	BioLegend	Cat# 506904 RRID: AB_315464
Mouse anti-IFN gamma APC	eBioscience	Cat# 17-7311-81 RRID: AB_469503
Mouse anti-CD19 Brilliant Violet 650	BioLegend	Cat# 115541 RRID: AB_11204087
Mouse anti- CD11b Brilliant Violet 605	BioLegend	Cat# 101237 RRID: AB_11126744

(*Continued on next page*)

Continued

REAGENT or RESOURCE	SOURCE	IDENTIFIER
Mouse anti-CD11c FITC	BioLegend	Cat# 117305 RRID: AB_313774
Mouse anti-mouse Ly-6G PE/Cy7	BioLegend	Cat# 127617 RRID: AB_1877262
Mouse anti-mouse F4/80 PerCP/Cy5.5	BioLegend	Cat# 123127 RRID: AB_893496
Mouse anti-Ly-6C Alexa Fluor 700	BioLegend	Cat# 128024 RRID: AB_893496
Mouse anti-PDCA-1 APC	BioLegend	Cat# 127015 RRID: AB_1967101
Mouse anti-mouse CD103 PE	BioLegend	Cat# 121405 RRID: AB_535948
Mouse anti-mouse Lineage Cocktail with Isotype Ctrl FITC	BioLegend	Cat# 133301 RRID: AB_10697030
Mouse anti-CD90.2 PerCP-Cyanine5.5	Tonbo Biosciences	Cat# 65-0903 RRID:N/A
Mouse anti-CD127 Brilliant Violet 605	BioLegend	Cat# 135025 RRID: AB_2562114
Mouse anti-RORgt APC	eBioscience	Cat# 17-6981-80 RRID: AB_2573253
Mouse anti-GATA3 PE	BioLegend	Cat# 653803 RRID: AB_2562722
Mouse anti-mouse NK-1.1 FITC	BioLegend	Cat# 156507 RRID: AB_2876526
Mouse anti-mouse CD8b FITC	BioLegend	Cat# 126605 RRID: AB_961293
Biological samples		
Healthy human colon biopsy	Boston children's hospital	N/A
Chemicals, peptides, and recombinant proteins		
Calcitonin Gene Related Peptide (CGRP)	GeneScript	Cat# 96827-03-1
Clozapine-N-Oxide	Tocris	Cat# 4936
recombinant mouse NGF	Thermo Fisher Scientific	Cat# A42627
Capsaicin	Tocris	Cat# 0462
Fura-2 AM	Thermo Fisher Scientific	Cat # F1221
Opal 520	Akoya Biosciences	Cat# FP1487001KT
Opal 570	Akoya Biosciences	Cat# FP1488001KT
Resiniferatoxin (RTX)	Alomone Lab	Cat #R400
BIBN 4096	Tocris	Cat #4561
Ultrapure BSA	Invitrogen	Cat #AM2616
Ulex Europaeus Agglutinin I (UEA I) Rhodamine	Vector Laboratories	Cat# RL-1062
Celltrace Calcein Violet	Thermo Fisher Scientific	Cat# C34858
Collagenase VIII	Sigma-Aldrich	Cat# C2139
Deoxyribonuclease I	Sigma-Aldrich	Cat# D5025
Fluospheres™ Polystyrene Microspheres, 1.0 μm, red fluorescent	Thermo Fisher Scientific	Cat# F13083
ALZET Osmotic Pump	Alzet	Cat# 1007d
Krebs-Ringer Solution	Alfa Aesar	Cat# J67795
DAPT	Sigma-Aldrich	Cat# D5942
IWP-2	Sigma-Aldrich	Cat# I0536
rmEGF	Peprotech	Cat# 31509
Collagen	Sigma-Aldrich	Cat# C5533

(*Continued on next page*)

Please cite this article in press as: Yang et al., Nociceptor neurons direct goblet cells via a CGRP-RAMP1 axis to drive mucus production and gut barrier protection, Cell (2022), https://doi.org/10.1016/j.cell.2022.09.024

Continued

REAGENT or RESOURCE	SOURCE	IDENTIFIER
TripLE	Life technology	Cat# 1265010
Carbachol	Sigma-Aldrich	Cat# Y0000113
Acridine Orange	Sigma-Aldrich	Cat# A6014
Critical commercial assays		
CGRP rat Enzyme Linked Immunosorbent Kit	Cayman Chemical	Cat# 589001
LIVE/DEAD™ Fixable Near-IR Dead Cell Stain Kit	Thermo Fisher Scientific	Cat# L34975
RNAscope® Probe- Hs-MUC2	Advanced Cell Diagnostics	Cat# 312871
RNAscope® Probe- Hs-RAMP1-C2	Advanced Cell Diagnostics	Cat# 483051-C2
RNAscope® Probe- Mm-Muc2-C2	Advanced Cell Diagnostics	Cat# 315451-C2
RNAscope® Probe- Mm-Ramp1-O1	Advanced Cell Diagnostics	Cat# 532681
RNAscope Multiplex Fluorescent Assay v2	Advanced Cell Diagnostics	Cat# 323110
RNAscope Multiplex Fluorescent Detection Kit	Advanced Cell Diagnostics	Cat# 320851
QIAamp DNA Stool Mini Kit	QIAGEN	Cat# 51504
Fixation/Permeabilization kit	BD	Cat# 554714
Transcription factor staining buffer set	eBioscience	Cat# 00-5523-00
Chromium Next GEM Single Cell 3' Reagent Kit v3.1	10X Genomics	Cat# CG000315
Chromium Next GEM Single Cell 3' Kit v3.1	10X Genomics	Cat# 1000268
Chromium Next GEM Chip G Single Cell Kit	10X Genomics	Cat# 1000120
Dual Index Kit TT Set A	10X Genomics	Cat# 1000215
Acridine Orange/Propidium Iodide stain	Logos Biosystems	Cat# F23011
Kapa qPCR Library Quantification Kit	Roche Sequencing Solutions	Cat# 07960140001
High Sensitivity D5000 Tape	Agilent Technologies	Cat#5067-5592
High Sensitivity D5000 Reagents	Agilent Technologies	Cat# 5067-5593
Deposited data		
Raw 16S sequencing	BioProject	PRJNA803622
$Nav1.8^{DTA}$ colonic epithelial cells	This paper	GSE208762
$Ramp1^{Villin}$ colonic epithelial cells	This paper	GSE208762
$Nav1.8^{DTA}$ ileal epithelial cells	This paper	GSE208594
Experimental models: Mouse strains		
Mouse: C57BL/6	Jackson Laboratory	Stock #000664
Mouse: B6.Rosa26-stop(flox)-DTA	Jackson Laboratory	Stock #009669
Mouse: B6.Rose26-stop(flox)-tdTomato	Jackson Laboratory	Stock #007914
Mouse: Calca-GFP-DTR	Provided by M. Zylca	McCoy et al., 2013
Mouse: B6.Cg-$Calca^{tm1.1(cre/EGFP)Rpa}$/J	Jackson Laboratory	Stock #033168
Mouse: Nav1.8-Cre	Provided by J. Wood	Abrahamsen et al., 2008
Mouse: $Calca^{-/-}$	Provided by V. Kurchroo	Oh-hashi et al., 2001
Mouse: $Calcb^{-/-}$	Provided by M. Rao	Thompson et al., 2008
Mouse: C57BL/6N $Ramp1^{tm1a(EUCOMM)Wtsi}$/H	EMMA	Stock #07401
Mouse: Villin1-Cre	Jackson Laboratory	Stock #018963
Mouse: B6N;129-Tg(CAG-CHRM3*,-mCitrine)1Ute/J	Jackson Laboratory	Stock #026220
Mouse: Germ free C57BL/6	Provided by J. Huh	N/A
Oligonucleotides		
EUB338 pan-eubacterial Cy-3 conjugated FISH probe	IDT	(5'-GCTGCCTCCCGTAGGAGT'3')
Nonsense Cy-3 conjugated FISH probe	IDT	(5'-CGACGGAGGGCATCCTCA-3')
Software and algorithms		
FlowJo V10	Treestar	www.flowjo.com
FIJI Is Just Image J version 2	ImageJ	https://fiji.sc

(*Continued on next page*)

Continued

REAGENT or RESOURCE	SOURCE	IDENTIFIER
QIIME version 1.9.1	Kuczynski et al., 2012	qiime.org
Intestine Explant Perfusion system	This paper	https://github.com/mdanderson03/mucus_explant
Mucus Quantification v8	This paper	https://github.com/prajuvikas/Mucus_Quantification_v8_2022Jan
Other		
Cytoflex S flow cytometer	Beckman Coulter	N/A
FACSAria	BD	N/A
Stellaris 8 FALCON CFS	Leica	N/A
Thunder 3D Cell Culture	Leica	N/A
Eclipse Ti-S/L100 inverted microscope	Nikon	N/A

RESOURCE AVAILABILITY

Lead contact

Please direct requests for resources and reagents to Lead Contact, Isaac Chiu (Isaac_Chiu@hms.harvard.edu).

Materials availability

This study did not generate new unique reagents.

Data and code availability

The accession number for the 16S sequencing data reported in this paper is Bioproject: PRJNA803622.

The accession numbers for the scRNA-seq data of intestinal epithelial cells reported in this paper are GEO: GSE208762 and GEO: GSE208594.

The code for mucus thickness quantification of ex vivo explant images can be found in the following repository: https://github.com/prajuvikas/Mucus_Quantification_v8_2022Jan (https://doi.org/10.5281/zenodo.7080173). The code has only been tested on the images generated in this study, and optimization will be needed for other image analysis. Any additional information required to reanalyze the data reported in this work paper is available from the lead contact upon request.

EXPERIMENTAL MODEL AND SUBJECT DETAILS

Mice

C57BL/6, B6.Rosa26-stop(flox)-DTA, Ai14 strain B6.Rosa26-stop(flox)-tdTomato, B6N;129-Tg(CAG-CHRM3*,-mCitrine)1Ute/J and Villin-Cre mice were purchased from Jackson Laboratories. Nav1.8-Cre mice were provided by J. Wood (University College London). Calca-GFP-DTR (McCoy et al., 2013) were provided by M. Zylka and E. McCoy (University of North Carolina). Calca$^{-/-}$ (Oh-Hashi et al., 2001) mice were provided by V. Kuchroo (Harvard Medical School). Calcb$^{-/-}$ (Thompson et al., 2008) mice were provided by M. Rao (Boston Children's Hospital). Germ-free mice were provided by J. Huh (HMS). Nav1.8-Cre$^{+/+}$mice were crossed with B6.Rosa26-stop (flox)-tdTomato mice to generate Nav1.8-lineage neuron labeled mice (Nav1.8^{tdTomato}) mice. For Nav1.8-lineage neuron depletion experiments, Nav1.8-Cre$^{+/-}$mice were crossed with Rosa26-stop(flox)-DTA$^{+/+}$ mice to generate Nav1.8-lineage neuron-depleted Nav1.8-Cre$^{+/-}$; DTA$^{+/-}$ (Nav1.8^{DTA}) mice and control Nav1.8-Cre$^{-/-}$; DTA$^{+/-}$ (Ctrl) littermates. For gut epithelial cell specific *Ramp1* depletion experiments, Villin-Cre$^{+/-}$;Ramp1$^{fl/fl}$ mice were bred to Ramp1$^{fl/fl}$ mice to generate mice with epithelial-specific depletion of Ramp1 in Villin-Cre$^{+/-}$;Ramp1$^{fl/fl}$ (Ramp1^{Villin}) or control (Ramp1$^{fl/fl}$) littermates. For Calca and Calcb deficient mouse experiments, heterozygous mice were bred together to produce wild-type and knockout littermates. For Nav1.8-lineage neuron activation experiments, Nav1.8-Cre$^{+/-}$mice were crossed with B6N;129-Tg(CAG-CHRM3*,-mCitrine)1Ute/J mice to generate Nav1.8-lineage neuron activation DREADD Nav1.8-Cre$^{+/-}$; hM3Dq$^{+/-}$ (Nav1.8^{hM3Dq}) mice and control Nav1.8-Cre$^{-/-}$; hM3Dq$^{+/-}$ (Ctrl) littermates. For Calca-lineage neuron activation experiments, Calca-Cre$^{+/-}$mice were crossed with B6N;129-Tg(CAG-CHRM3*,-mCitrine)1Ute/J mice to generate CGRP-lineage neuron activation DREADD Calca-Cre$^{+/-}$; hM3Dq$^{+/-}$ (Calca^{hM3Dq}) mice and control Calca-Cre$^{-/-}$; hM3Dq$^{+/-}$ (Ctrl) littermates.

Mice were bred and housed in a specific pathogen-free animal facility at Harvard Medical School (HMS). Age-matched 6- to 12-week-old littermate male and female mice were used for experiments. All animal experiments were approved by the HMS Institutional Animal Use and Care Committee.

Human intestinal tissue samples

Healthy human transverse colon biopsy tissue was obtained from a 20-year-old female patient and human splenic flexure biopsy tissue was obtained from a 10-year-old male patient, respectively, during diagnostic colonoscopy as part of routine clinical care

Please cite this article in press as: Yang et al., Nociceptor neurons direct goblet cells via a CGRP-RAMP1 axis to drive mucus production and gut barrier protection, Cell (2022), https://doi.org/10.1016/j.cell.2022.09.024

under approved Boston Children's Hospital Institutional Review Board Protocol P00027983. Biopsy samples were fixed in 10% Neutral Buffered Formalin, embedded in paraffin, and cut into 5-7μm sections for staining.

METHOD DETAILS

DRG isolation and culture

Mice were euthanized and DRGs were dissected and dissociated as previously described (Pinho-Ribeiro et al., 2018). DRG neurons were plated on laminin pre-coated 35mm culture dishes (2,000 cells/dish) in 50 ng/ml NGF in neurobasal media (ThermoFisher) and used for calcium imaging 24-48h after plating. For calcium imaging, cells were pre-loaded with Fura2-AM (5mM) in neurobasal media at 37 °C for 30 min. Cells were washed twice and imaged in 2 ml Krebs buffer (Krebs-Ringer solution). After the addition of stimuli described below, images were acquired with alternating 340/380 nm excitation wavelengths, and fluorescence emission was captured using a Nikon Eclipse Ti inverted microscope. Ratio metric analysis of 340/380 signal intensities were processed, background corrected, and analyzed with NIS-elements software (Nikon) by drawing regions of interest (ROIs) around individual cells. Responses were measured as $\Delta F/F_0 = [(F - F_0)/F_0]$, where F is the peak fluorescence signal and F_0 is the mean fluorescence signal at baseline. Peak responses were included in the analysis if the response was 5 SDs above baseline. The percentage of responsive cells was quantified and plotted for the stimulus in question as a percentage of total (KCl responsive) neurons.

For fecal supernatant induced neuron activation, DRGs from wildtype B6 mice were cultured as above. Two fecal pellets from SPF or GF mice were collected, mashed, and resuspended in 1 ml Krebs-Ringer buffer. After filtering with a 70 μm cell strainer, the fecal mixture was centrifuged at 12000g for 10 minutes at 4 °C and the supernatant was collected for cell stimulation. After 10 min. of fecal supernatant or vehicle treatment, 1 μM capsaicin (Tocris) and 40 mM KCl (Sigma) were applied sequentially to identify TRPV1+ and live neurons, respectively.

For *Nav1.8*$^{+}$ neuron activation, DRGs from Nav1.8^{hM3Dq} and control mice were cultured as above. Krebs-Ringer solution (vehicle), 0.1nM CNO or 1nM CNO was applied for 2 minutes. After vehicle or CNO application, 1 μM capsaicin and 40 mM KCl were applied sequentially to identify neuron activation as a percentage of live neurons.

CGRP release of DRG neuron cultures, colonic explants, and serum

DRG neurons were cultured as described above in a 96 well plate (5,000 cells per well) for one week. Media was aspirated and replaced with 200 μl fresh neurobasal media prior to stimulation. DRG neurons from wildtype B6 mice were stimulated with 1 μl fecal supernatant or 1 μM capsaicin for 1 hour at 37 °C with 5% CO2. DRG neurons from Nav1.8^{hM3Dq} and control mice were stimulated with 1 nM CNO or vehicle for 1 hour at 37 °C with 5% CO2. 100 μl culture supernatant was collected for CGRP concentration measurement using a CGRP EIA Kit (Cayman Chemicals).

For CGRP release from colonic explants, distal colons (3 cm each) from SPF, GF, SPF fecal-transplanted GF mice pre-treated with or without resiniferatoxin (RTX), and antibiotic-treated and untreated Nav1.8^{DTA} and control mice were dissected and transferred into 24 well plate containing 500 μl DMEM. Explants were incubated for 1 hour at 32 °C with gentle shaking at 150 rpm. 100 μl explant culture supernatant was collected for CGRP concentration measurement using a CGRP EIA Kit (Cayman Chemicals). For antibiotic treatment, mice were treated with a cocktail of ampicillin (1 mg/ml), vancomycin (0.5 mg/ml), metronidazole (1 mg/ml), and neomycin (1 mg/ml) in the drinking water for three weeks.

For CGRP release in serum, blood was collected from naïve Nav1.8^{DTA} and control mice, and CNO-treated Calca^{hM3Dq} and control mice and centrifuged at 3000 rpm for 10 min. after coagulation. 50 μl serum was collected for CGRP concentration measurement using a CGRP EIA Kit (Cayman Chemicals).

3D colonoid and 2D primary epithelial cell culture

Colonic organoids were derived from isolated crypts collected from the large intestine of wildtype C57BL/6J mice as previously described (Sato et al., 2011). Approximately 500 crypts were plated in a 50 μl drop of Matrigel in 24-well plates and overlaid with 500 μl of WENR medium, containing basal crypt media (Advanced DMEM/F12, penicillin/streptomycin, 10 mM HEPES, 2 mM Glutamine), supplemented with 1× B27 (Gibco, 17504-044), 1× N2 (Gibco,17502-048), 50 ng/ml rmEGF (Peprotech, 315-09), 50% L-WRN-CM (conditioned medium) (v/v), 10 μM Rock inhibitor Y-27632 (Sigma, Y0503), 3 μM CHIR99021 (Sigma, SML1046) with a final FBS concentration of 10%. Media was changed every 2 days and colonoids were split every 4 days. Cultures were passaged three times prior to experiments. For 2D monolayer cultures, colonoids were extracted from Matrigel with organoid harvesting solution (R&D system, 3700-100-01), and then digested with undiluted TripLE (Life Technologies, 1265010). Colonoid fragments were suspended in WENR medium and plated on collagen-coated (Sigma, C5533) 35mm glass bottom dishes (Cellvis, D35-20-1.5-N). To enrich primary epithelial cultures toward goblet cells, 12h after seeding, the media was changed into secretory cell differentiation medium containing basal crypt media (Advanced DMEM/F12, penicillin/streptomycin, 10 mM HEPES, 2 mM Glutamine), supplemented with 1× B27 (Gibco, 17504-044), 1× N2 (Gibco,17502-048), 50 ng/ml rmEGF (Peprotech, 315-09), 100ng/ml Noggin (Peprotech 250-38), 10% R-spondin1-CM (conditioned medium) (v/v), 10 μM g-Secretase Inhibitor DAPT (Sigma, D5942), 2 μM Wnt pathway inhibitor IWP-2 (Sigma, I0536) with a final FBS concentration of 10%. Media was changed on day 2 and differentiated cell monolayers were ready for experiments on day 4.

For granule release measurements, the cultured cells were preloaded with 10 mM Acridine Orange (AO) for 10 minutes and then treated with vehicle, CGRP (100ng/ml), or Carbachol (1μM) for 15 minutes and imaged in real-time on a widefield microscope (Thunder 3D Cell Culture, Leica) at 20X every 5 minutes. 2-5 areas from each dish were imaged and each area contained 100-200 cells. The total area of granules per cell was measured using FIJI. For intracellular MUC2 staining, the cultured cells were treated with vehicle, CGRP (100ng/ml), or Carbachol (1μM) for 15 minutes, and then fixed with 4% PFA, permeabilized with 0.1% Triton X-100 and stained for MUC2 as described below. The stained cells were imaged using a confocal microscopy at 63X and the intensity of MUC2 per cell were analyzed in FIJI.

Immunostaining of mucin

In vivo mucus layer thickness analysis was performed as described (Johansson and Hansson, 2012). Briefly, mice were euthanized and tissue from the distal $^1/_3$ of the colon with fecal pellets was removed and fixed for 24-48h in methanol-Carnoy's fixative at room temperature. Tissues were processed and paraffin-embedded without exposure to water to maintain mucus layer structure and integrity. 5 μm tissue cross-sections were heated at 60 °C for 10 min prior to incubation in xylene twice for 10 min, and then rehydrated with decreasing concentrations of ethanol (100, 95, 70, 50 and 30%) for 5 min each at room temperature. Antigen retrieval was performed by steaming samples in antigen retrieval solution (10 mM citric buffer, pH 6.0) for 15min and leaving samples in warm solution for an additional 20min. Samples were washed in PBS and blocked with 5% FBS in PBS for 30 minutes at 4 °C. Samples were stained for the mucus layer using an anti-MUC2 primary antibody and fluorescent secondary antibody. For FISH staining, sections were stained overnight at 50 °C with either 1 μg/ml nonsense control or eubacterial probe in hybridization buffer (20 mM Tris-HCl pH 7.4, 0.9M NaCl, 0.1% SDS, 0.5% formamide). Slides were incubated in FISH washing buffer (20 mM Tris-HCl pH 7.4, 0.9 M NaCl) at 50 °C for 10 mins, and then washed 3 times in PBS at room temperature. Samples were stained with DAPI, mounted with Prolong Antifade mounting medium, and sealed prior to imaging. Sections were imaged on a widefield microscope and mucus layer thickness was measured using FIJI. At least 20 measurements per tissue cross-section from at least 3 cross-sections were collected to determine average mouse mucus thickness measurements. Analysis was blinded.

Immunostaining of goblet cells

For microscopy analysis of goblet cell numbers and goblet cell maturation, mice were euthanized and ileum or distal colon pieces without fecal content were collected and fixed in either 4% PFA or methanol-Carnoy's fixative for at least 24 hours at room temperature. Tissues were processed, paraffin-embedded, and cut into 5 μm sections. Tissue sections were processed as above for mucus layer analysis, blocked for 2 hours with 2% normal donkey serum, stained for MUC2 using an anti-MUC2 primary antibody and a fluorescent-conjugated secondary antibody. For goblet cell maturation staining, sections were additionally stained with fluorescent-conjugated UEA-1 (1μg/ml) during the secondary antibody staining. Samples were washed in PBS, stained with DAPI, and mounted prior to imaging. Sections were imaged on a confocal microscope and goblet cells per crypt were counted using FIJI. At least 10 full crypts were measured per to determine goblet cell numbers and maturation. Analysis was blinded.

H&E and AB/PAS staining analysis

For Ramp1 signaling blockade *in vivo*, the Calca^{hM3Dq} and control mice were pretreated with either vehicle or BIBN4096 (0.3 mg/kg) by i.p. injection for 30 minutes. 10 minutes prior to euthanization, mice were treated with CNO (1 mg/kg) by i.p. injection. For CGRP injection, mice were treated with CGRP (10 μg/mouse) by i.p. injection for 10 minutes. Mice were euthanized and colon tissues were collected and fixed in 4% PFA for at least 24 hours prior to H&E (hematoxylin and eosin) and AB/PAS (Alcian blue/Periodic acid-Schiff) staining. Whole cross-sections were scanned and imaged on a widefield microscope at 20X.

For H&E staining, images were analyzed using a scoring system as previously described (Koelink et al., 2018). Briefly, cross-sections were randomly split into 8 sections and 4 random sections were scored qualitatively using a 0-3 point scale for infiltrate, goblet cell loss, crypt density, crypt hyperplasia, muscle thickening, submucosal infiltrate, ulceration, and abscess. Scores from each item were combined for a composite score for each mouse. Scores from each section were averaged for each mouse. Scoring was performed blinded.

For AB/PAS staining intensity analysis, images were loaded into FIJI. After color deconvolution, Periodic acid-Schiff staining was converted to Lut-Grey-scale, inverted, and intensity measurement made. Goblet cell mucus content was determined by measuring the intensity of PAS signal in an individual full crypt in at least 20 crypts per section. Analysis was blinded.

RNAscope

For mouse *Muc2* and *Ramp1* RNAscope staining, ileums and colons were collected, embedded in OCT and frozen. 14μm sections were fixed with 4% PFA at 4 °C for 15 min and stained for *Muc2* and *Ramp1* using the RNAscope Multiplex Fluorescent Detection Kit (Advanced Cell Diagnostics) following the manufacturer's instructions. Entire sections were imaged using a confocal microscopy at 20X and images were analyzed in FIJI.

For human *MUC2* and *RAMP1* RNAscope staining, 5 μm paraffin-embedded sections were deparaffinized, treated with hydrogen peroxide for 10 minutes, and boiled in RNAscope Target retrieval buffer for 15 minutes. The sections were then stained for *MUC2* and *RAMP1* using RNAscope Multiplex Fluorescent Assay v2 (Advanced Cell Diagnostics) following the manufacturer's instructions. Entire sections were imaged using a confocal microscopy at 20X and images were analyzed in FIJI.

Please cite this article in press as: Yang et al., Nociceptor neurons direct goblet cells via a CGRP-RAMP1 axis to drive mucus production and gut barrier protection, Cell (2022), https://doi.org/10.1016/j.cell.2022.09.024

Ex vivo mucus analysis

Colon tissues were collected for explant culture and mucus imaging as previously described (Gustafsson et al., 2012). Briefly, the distal colon was collected, flushed with ice-cold oxygenated Kreb's buffer and opened along the mesenteric border. After removal of the longitudinal muscle layer, the explant was mounted in a custom-made imaging perfusion chamber (https://github.com/mdanderson03/mucus_explant) where the apical chamber filled with Kreb's buffer containing D-mannitol (10 mM) and the basolateral chamber was perfused with Kreb's buffer containing D-glucose (10 mM) plus Celltrace Calcein Violet (Thermo Fisher) at a rate of 2 ml/min. 10 μl 1-μm-diameter fluorescent beads were gently added to the apical surface. The beads and explants were imaged in XY stacks (550 μm x 550 μm) using a Stellaris 8 FALCON CFS microscope (Leica) at a step size of 10 μm. Consistent with published studies, our approach relies on flushing the intestinal lumen prior to explant preparation, leading to removal of looser luminal mucus in our studies.

For CGRP-induced mucus growth analysis, the basal mucus layer on the explant surface was gently removed by cotton swabs under a dissection scope before mounting into the chamber. CGRP (100 ng/ml) was added into perfusion buffer, and the mucus growth was recorded for 30 minutes. 3∼5 fields from each explant were captured for the following analysis.

The relative distribution of beads to colonic explant surface was measured in ImageJ (https://github.com/prajuvikas/Mucus_Quantification_v8_2022Jan) for mucus thickness analysis. Briefly, the distances of the lowest beads to the surface of explant after tissue smoothening were measured. The mucus thickness of each field was measured by the mode distance of the lowest beads (see Video S1).

Whole mount immunostaining

Mice were euthanized and perfused with 30 ml PBS, and distal colons and distal ileums were collected for staining. Colons with intact mesenteric nerves were dissected for immunostaining of extrinsic innervation. The intestines were opened and fixed in a Silgard dish with 4% PFA at 4°C overnight. After blocking, tissues were dissected into small pieces (3 mm x3 mm) and incubated with primary antibody (rabbit anti-MUC2, 1:500; rat anti-EpCAM, 1:500; rabbit anti-CGRP, 1:500; goat anti-mCherry, 1:500; chicken anti-GFP, 1:500; rabbit anti-Tyrosine Hydroxylase, 1:500; UEA-1, 1:1000) in PBST (1% Triton-X100/PBS) for 3 days followed by secondary antibody staining in PBST for 2 days. After dehydration with serial (50%, 80%, 100%) methanol solution and clearing in BABB buffer (1 volume Benzyl Alcohol to 2 volume Benzyl Benzoate), the pieces were mounted on glass slides using vacuum grease for imaging. Three different fields of each tissue were imaged with a 1 μm z-stack step size and 3D image was built in Stellaris 8 FALCON CFS system (Leica).

Intestinal epithelial cell and immune cell isolation

Intestinal epithelial cells were isolated as previously described (Jarret et al., 2020). Briefly, distal colon and distal ileum were collected from euthanized mice and flushed with ice cold PBS. Colons and ileums were cut into 0.5cm pieces and incubated on ice for 5 min in 10 mL of PBS containing 5 mM EDTA and 1 mM DTT. After shaking, the intestinal pieces were incubated at 37 °C for 10 minutes in PBS containing 5 mM EDTA and 2% FBS. After vigorous shaking, the wash containing crypts was collected. This step was performed three times in total for colonic pieces and two times for ileal pieces with the epithelial fraction collected at the end of each wash. The crypt cells were pelleted and digested with 10 ml HBSS containing 8 mg Dispase II (Sigma) for 10 minutes at 37 °C. Single epithelial cells were collected in PBS containing 2% FBS for flow cytometry staining.

For lamina propria immune cell isolation, colonic pieces after removal of crypts as described above were digested in 10 mL of RPMI containing 2% FBS, 1 mg/ml Collagenase VIII (Sigma) and 100 U/ml DNase I (Sigma) for approximately 60 min at 37 °C with shaking. The digested tissue was filtered by a 40 μm strainer and subjected to Percoll (GE) separation using an 80% and 40% gradient. Immune cells were harvested from the interphase of the Percoll gradient after a spin at 2500 rpm for 20 min at 4 °C. Cells were re-suspended in PBS containing 2% FBS for flow cytometry staining.

For intraepithelial lymphocytes (IELs) isolation, the wash containing crypts and IELs as described above was pelleted and subjected to Percoll gradient. IELs were collected from the interphase after centrifuge. Cells were resuspended in PBS containing 2% FBS for flow cytometry staining.

Flow cytometry

Cells isolated above were stained with surface antibody at 1:250 on ice for 20 minutes in flow buffer (2% FBS, 2 mM EDTA in PBS) and washed twice with flow buffer. For intracellular staining (mouse anti-IL17A PE, mouse anti-IFN gamma APC or rabbit anti-MUC2), cells were permeabilized and stained using a Fixation/Permeabilization kit (BD) according to the manufacturer's instructions. For transcription factor staining (mouse anti-FOXP3 Alexa Fluor 488, mouse anti-RORgt APC, mouse anti-GATA3 PE), a Transcription factor staining buffer set (eBioscience) was used according to the manufacturer's instructions. Data were acquired on a Cytoflex S flow cytometer (Beckman Coulter) and analyzed in Flowjo v10. Single epithelial cells ($CD45^{-}EpCAM^{+}$) were sorted by FACSAria (BD) and resuspended HBSS containing 0.01% BSA (Ambion #AM2616) for downstream single cell sequencing.

ILC depletion

ILCs were depleted as previously reported (Sonnenberg et al., 2012). Briefly, mice were treated twice with anti-CD90.2 mAb (BioXCell) every three days at a dose of 300 μg/mouse and used for the following experiments one week after injection.

Please cite this article in press as: Yang et al., Nociceptor neurons direct goblet cells via a CGRP-RAMP1 axis to drive mucus production and gut barrier protection, Cell (2022), https://doi.org/10.1016/j.cell.2022.09.024

10X scRNA-seq of colon

scRNA-seq of colonic epithelial cells isolated from Nav1.8^{DTA}, Ramp1^{Villin} and littermate control mice was performed using 10x Genomics Chromium Next GEM Single Cell 3' Reagent Kit v3.1 (10X genomics) following the user guide. Briefly, cells were counted on the LUNA-FX7 Automated Cell Counter (Logos Biosystems) using fluorescence detection for viability with an acridine orange/propidium iodide stain (Logos Biosystems). All samples had viability greater than 88% with concentration ranges from ~700-900 cells/μL. After counting, all samples were loaded into Chip G per the user guide from 10x Genomics. GEMs (Gel Beads-in-emulsions) were formed targeting 10,000 cells for each sample followed by immediate reverse transcription. The cDNA was cleaned from the GEM reagents, amplified for a total of 11 cycles and verified via TapeStation (Agilent Technologies). Amplified cDNA was diluted 1:6 and run on the 4200 TapeStation instrument using High Sensitivity D5000 tape and reagents (Agilent Technologies). The amplified cDNA was fragmented, end repaired, and A-tailed followed by adaptor ligation, and PCR amplification was run for a total of 11 cycles with each sample receiving a unique set of dual indices. Final libraries were diluted 1:10 and ran using the High Sensitivity D5000 tape and reagents on the 4200 TapeStation (Agilent Technologies). Libraries were quantified via Kapa qPCR using the Complete Universal Kit (Roche Sequencing Solutions) and the CFX96 Touch Real-Time PCR Detection System (Bio-Rad Laboratories). Libraries were sequenced on an Illumina NovaSeq S4 flow cell across one single lane (estimated reads per cell ~55,000) using the parameters outlined in the user guide (Read1: 28 bp, i7 index: 10 bp, i5 index: 10 bp, Read2: 90 bp). After sequencing, Cell Ranger count QC summary report identified between 12,000-14,000 single cells in the samples.

inDrops scRNA-seq of ileum

scRNA-seq of ileal epithelial cells isolated from Nav1.8^{DTA} (three mice pooled together) and their littermate control (three mice pooled together) mice was performed using inDrops single cell sequencing following the user guide. Briefly, cells were encapsulated in droplets following a previously described protocol (Klein et al., 2015; Zilionis et al., 2017), with the following modifications in the primer sequences. RT primers on hydrogel beads-

5'CGATTGATCAACGTAATACGACTCACTATAGGGTGTCGGGTGCAG [bc1,8nt] GTCTCGTGGGCTCGGAGATGTGTATAAGAG ACAG[bc2,8nt]NNNNNNTTTTTTTTTTTTTTTTTTV- 3'
PCR primer sequences (steps 157 and 160 in the library prep protocol in (Zilionis et al., 2017))-
5'-AATGATACGGCGACCACCGAGATCTACACXXXXXXXXTCGTCGGCAGCGTC-3', where XXXXXX is an index sequence for multiplexing libraries.
5'- CAAGCAGAAGACGGCATACGAGATGGGTGTCGGGTGCAG-3'

With these modifications in the primer sequences, custom sequencing primers are no longer required. The library prep protocol used here was based on Smart-seq2 (Picelli et al., 2014) with modifications. The workflow of the library preparation can be summarized as follows: Reverse transcription with Maxima H minus RTase at 50°C for 60 min -> cleanup with SILANE beads -> template switching reaction with Maxima H minus RTase -> SPRI purification -> cDNA amplification -> SPRI purification -> DNA fragmentation, end repair and A-tailing -> adapter ligation -> SPRI purification -> library enrichment PCR -> double-sided SPRI purification. Referring to the detailed protocol in (Picelli et al., 2014), the following modifications were made to the protocol: Reverse transcription and template-switching were decoupled, where reverse transcription occurred within the droplet, while template-switching was not. cDNA was fragmented enzymatically here followed by adapter ligation, as opposed to tagmentation in (Picelli et al., 2014). Sequence of the adapters are as follows- 5'-CTGTCTCTTATACACATCTGACGCTGCCGACGA- 3' (with 5' phosphorylation)
5'-AGATGTGTATAAGAGACAG*T- 3' (with phosphorothioate bond on the 3' terminal nucleotide). The barcoded library was sequenced as described above.

TRPV1 nociceptor neuron ablation

Systemic nociceptor neuron was ablated as previously described (Lai et al., 2020). Briefly, 4-week-old C57BL/6 mice were anesthetized with isoflurane and injected subcutaneously in the flank with escalating doses (30, 70, 100 μg/kg on consecutive days) of resiniferatoxin (RTX, Alomone Lab) or vehicle (2% DMSO/0.15% Tween-80/PBS). Mice were allowed to rest for 4 weeks before experiments. Loss of nociceptor neurons was confirmed by reduced thermal responses to noxious heat during hot plate tests (55 °C).

DSS-induced colitis

Briefly, 6- to 12- week-old gender-matched mice were given dextran sodium sulfate (DSS) (MP Biomedicals) in drinking water for the indicated days, followed with regular water. All mice were treated with 3.5% DSS, with exception of Ramp1^{Villin} and their littermate control mice which were treated with 2.5% (Figures 6K–6O, S7G, and S7H) and 3.5% DSS (Figures S7E and S7F). The mice were weighed daily and sacrificed on the indicated time points. Colon tissues were obtained for histopathological analysis.

Gut permeability assay

A gut permeability assay was performed as previously described (Nalle et al., 2019). Briefly, mice were fasted for 3 hours before oral gavage of 600 mg/kg FITC–4-kDa dextran (Sigma). Serum was collected 4 hours after gavage and analyzed using a Synergy HT plate reader (Bio-Tek) with 485 nm excitation and 528 nm emission.

Please cite this article in press as: Yang et al., Nociceptor neurons direct goblet cells via a CGRP-RAMP1 axis to drive mucus production and gut barrier protection, Cell (2022), https://doi.org/10.1016/j.cell.2022.09.024

Osmotic pump implantation

Mice were anesthetized by isoflurane and the skin between the scapulae was shaved. A small incision (0.5 cm in length) was made in the skin between the scapulae, and a small pocket was formed by spreading the subcutaneous connective tissue apart using a forceps. The osmotic pump (Alzet) filled with CGRP (10 μg/day) or vehicle was inserted into the pocket. Following implantation, the skin incision was closed with surgical glue.

Visceromotor response (VMR) assay

Visceral pain was measured by visceromotor response to colorectal distension (CRD) as previously described (Larauche et al., 2010). Briefly, a miniaturized pressure sensor and a custom-made balloon (1 cm × 2 cm) was tied together with a pressure transducer catheter (825-0101 Mikro-Cath; Millar Instruments) to form a ''balloon-pressure sensor''. After calibration under certain pressures and lubrication, the ''balloon-pressure sensor'' was inserted into the colorectum of anesthetized mice placed in a mouse restrainer. Three rounds of serial pressures (15, 30, 45, and 60 mmHg, 10 s duration, 4 min interval) was administered to each mouse followed by three repeated noxious colorectal distensions at 60 mmHg (10 s duration, 4 min interval) using a barostat (Distender Series IIR; G&J Electronics Inc), and voltage output was then converted to pressure using the digital analog convertor (Micro 3-1401; Cambridge Electronic Design) and Spike 2 software (CED, Ltd.). The VMR was calculated by the increase of intraluminal colonic pressure in response to CRD in Spike 2.

16S rDNA sequencing and data analysis

To analyze the microbiome of colon lumen contents, 2-3 colon pellets from each mouse were collected and frozen at -20 °C until use. To collect colonic mucosal scrapings, colons were longitudinally opened in a sterile dish and scraped with 1 ml PBS. Bacterial genomic DNA from frozen stool samples was extracted using QIAamp DNA Stool Mini Kit (QIAGEN). Purified DNA was quantified by Qubit dsDNA HS Assay (Thermo Fisher Cat# Q32854) and normalized. Amplicons were purified and quantified by Qubit dsDNA HS Assay and combined with equal mass to make a pooled library. The pooled library was multiplexed sequenced (Illumina MiSeq, 251 nt x 2 pair-end reads with 12 nt index reads) through the Harvard Biopolymer's Facility. Raw sequencing data were processed with QIIME2. In brief, raw sequencing data were imported to QIIME2 and demultiplexed, then DADA2 was used for sequence quality control and feature table construction. The feature table was used for beta diversity analysis, taxonomic analysis, and differential abundance testing using QIIME2. Beta group significance was determined by permutational analysis of variance (PERMANOVA). Identification of taxa associated with different groups was determined using Analysis of Composition of Microbiomes (ANCOM).

Western blot of MUC2

Mucus samples were collected by scraping as described above. After quantification by BCA protein assay (Thermo Scientific cat#23227), equal amounts of protein were enriched by methanol and chloroform precipitation and resuspended with 1X Laemmli buffer (Bio-Rad) followed by incubation on a 95° heat block for 10 minutes. Samples were loaded on Bolt 4-12% Bis-Tris-Plus gels (Thermo Scientific cat# NW04125BOX), and gels were transferred to nitrocellulose iBlot 2 membranes (Fisher Scientific cat# IB23001), blocked with 5% Pierce Clear Milk Blocking Buffer (Thermo Scientific cat# 37587) for 30 minutes, washed 3x with TBST (TBS, 0.05% Tween-20), and incubated in blocking buffer containing MUC2 antibody (1:500) at 4° overnight. After washing 3x with TBST for 10 min, membranes were incubated with IR-fluorophore conjugated secondary antibody (LI-COR Biosciences cat# 926-32213) for 1h at RT, followed by three additional 10 min washes with TBST and imaged on a Li-COR imaging system.

QUANTIFICATION AND STATISTICAL ANALYSIS

For all quantifications, the exact value of n is described in detail in the Figure legends, where n indicates biological replicates, either number of mice, number of wells containing cells or number of areas containing cells. For all microscopy analysis, images were blinded prior to scoring and quantification. All statistical analyses were performed using Microsoft Excel and GraphPad Prism software. Data were represented as mean ± standard error (SEM) throughout the Figures and the level of significance was indicated by asterisks for the following corresponding p-values: *p <.05, **p <.01, ***p <.001, ****p <.0001. The specific statistical test used to for each experiment is described in detail in the Figure legends. For comparisons between two groups, we performed student's two-sided t-tests, except for non-parametric analysis of mucus thickness per measurement, where we utilized Mann-Whitney tests. For comparisons that have more than two groups or two conditions, One-way ANOVA and Two-way ANOVA were utilized. Multiple t-tests were used to determine the significance of water consumption and body weight analysis. For survival data, Log-rank test was used. No specific methods were utilized to determine whether data met assumptions of specific statistical approaches. Sample sizes for all experiments were chosen according to standard practice in the field.

Single-cell RNA-seq data analysis

Quality control and normalization of scRNA-seq data

The unique molecular identifier (UMI) count matrices obtained from the Cell Ranger output were imported into R (v.4.0.3) and processed with the R package Seurat (v. 4.1.0) (Hao et al., 2021). Low-quality cells were removed based on the following criteria. (i) Cells

with relatively high mitochondrial percentage were removed. For the colonic epithelial cell data (i.e., Nav1.8^{DTA}, Ramp1^{Villin}), all the cells with mitochondrial reads > 25% were excluded. For the Ileum data (Nav1.8^{DTA}), all the cells with mitochondrial reads > 10% were removed. (ii) The thresholds for acceptable numbers of detected genes and UMIs per cell were determined by outliers in the joint distribution of unique UMIs and detected genes across cells. For the Nav1.8^{DTA} colon data, cells with < 1200 or > 7400 detected genes were discarded. For the Ramp1^{Villin} colon data, cells with < 3000 or >7500 detected genes were discarded. For the ileum data, cells with < 500 or > 3000 detected genes were discarded. For the Nav1.8^{DTA} colon data, cells with < 4000 or > 70000 detected UMIs were discarded. For the Ramp1^{Villin} colon data, cells with < 14000 or > 50000 detected UMIs were discarded. For the Ileum data, cells with < 650 or > 9500 detected UMIs were discarded. To account for differences in sequencing depth across cells, UMI counts were normalized and scaled using regularized negative binomial regression via Seurat's sctransform() function (Hafemeister and Satija, 2019). In the case of the Ileum data, the batch effect for the three replicates was removed using the "vars.to.regress" argument as part of the sctransform() function. The resulting corrected counts were used for visualization and clustering downstream analysis.

Clustering and identification of cell type markers

We performed principal component analysis (PCA) using the top 3000 highly variable genes. The top 15 principal components for each dataset were used to construct a shared nearest neighbor (SNN) graph and modularity-based clustering using the Louvain algorithm and a cluster resolution of 0.1 as part of the FindClusters() function from the R package Seurat. Uniform manifold approximation and projection (UMAP) visualization was calculated using 15 nearest neighbors for the local approximation of the manifold structure. To annotate the cell types of each cluster, FindAllMarkers() was run with the option "test.use = LR", which identifies marker genes by comparing expression of each gene in a cluster against its expression in the rest of the cells using a logistic regression test. Only genes significantly and strongly up-regulated in the cluster were considered as potential markers. Potential markers were then intersected with canonical markers from the literature for intestinal epithelial cells (Haber et al., 2017), and the results were used to annotate the clusters of the colon and ileum samples (Figures S2A, S2B, and S4L; Table S1).

Differential expression analysis

To test whether genes were statistically differentially expressed (DE) between mouse genotypes within specific cell types, a negative binomial generalized linear model in the DESeq2 (v.1.30.1) R package was used via the Seurat wrapper function FindMarkers() with option "test.use=DESeq2". For each cell type being tested, the input consisted of the subset of the count matrix containing the cells annotated by that cell type. Size factors and dispersions were estimated prior to fitting the model. Wald statistics were used to determine the significance and the LFC of the fit for each gene. Benjamini-Hochberg method was used to control the false discovery rate (FDR). The differentially expressed genes used in subsequent analysis was determined using an FDR threshold of < 0.05 and an absolute $\log_2$ fold change (LFC) of > 0.2 (Tables S2–S4). P values reported in figures are FDR adjusted (Figures 5F, S4C, and S4G).

Gene set enrichment analysis

DE genes in each cell type were subject to gene set enrichment analysis using the "biological processes" set from the gene ontology database (GO). Specifically, enrichment analysis was performed using the enrichGO() function from the R package clusterprofiler (Yu et al., 2012), with the universe defined as the set of genes expressed in each respective dataset. Further, the upregulated and downregulated pathways were calculated using upregulated and downregulated DE genes respectively. Enriched pathways (i.e., $P < 0.05$) were collapsed to independent pathways to avoid repetition using clusterprofiler's simplify() function (Figures S5E and S5G; Table S5 and S6). For plots of enriched pathways of interest (Figures 5G, 5I, S4N, and S5B), the average expression shown for a given cell type and mouse model is computed as the average expression of the genes that are DE between mouse genotypes in that cell type and contained in the enriched pathway.

Single-cell data visualization

All plots illustrating gene expression levels use SCT transformed expression. Dot plots (Figures 5H, 5J, S5A, S5F, and S5H) show the z-scored expression across conditions; any values outside the range shown in the numerical legend were squished towards the maximum or minimum values shown. Violin plots (Figures 5G, 5I, S4D, S4I, S4N, S5B, and S5C) use a multiplicate bandwidth adjustment of 1.5.

Mass spectrometry-based mucus proteomics

Mucus sample preparation

The mucus proteins were prepared as described above and loaded onto a Bolt 4-12% Bis-Tris-Plus gels (Thermo Scientific) to run for 10 minutes. Gel pieces containing proteins were cut for digestion. The mucus proteins were in-gel digested according to a previous published protocol with modifications (Shevchenko et al., 2006). Briefly, gel pieces containing proteins were transferred to Eppendorf tubes and mashed into small pieces. The pieces were incubated in 500 μL of acetonitrile for 10 min until shrunk. The shrunk pieces were incubated in 50 mM dithiothreitol (Roche) in 50 mM ammonium bicarbonate at 56 °C for 30 min, washed with 500 μL acetonitrile, incubated in 100 mM iodoacetamide in the dark at room temperature for 20 min, and washed with 500 μL acetonitrile. The gel pieces were then incubated with 60 μL of 50 mM ammonium bicarbonate solution of trypsin/LysC (MS grade, Promega) at 4 °C for 90 min and 37 °C overnight. The protease to protein ratio was roughly 1:50. The liquid in the tubes were collected before gel pieces were eluted by 100 μL of 66.6% acetonitrile in 0.1% formic acid. The solutions were combined and concentrated with a SpeedVac (Sigma).

Mass spectrometry

The concentrated solutions were diluted to roughly 30 μL by 0.1% formic acid and 2 μL of the solution was injected into an Ultimate 3500 series nanoLC coupled to an Q Exactive mass spectrometer. A two-solution (solution A: 0.1% formic acid; solution B: 80% acetonitrile, 0.1% formic acid) nanoLC gradient (300 nL/min flow rate) was used to elute an Acclaim™ PepMap™ C18 column (2 μM, 75 μM, 15 cm, Thermo fisher): 1% B until 8 min, 1-9% B in 1 min, 9-11.5% B in 30 min, 11.5-23% B in 50 min, 23-30% B in 15 min, 30-35% B in 5 min, 50-80% B in 1 min and B was kept at 80% for 2 min before dropping back to 1% in 1 min and B was kept at 1% for 7 min.

The mass spectrometer was operated under the positive mode. The spray voltage was 1850 V. The ion transfer line temperature was 275 °C. MS resolution was set to 70 K and the mass range was 375-1500 Da. The maximum injection time was 60 ms. The AGC target was 1e6. S-lens RF level was 50. MSMS resolution was 17.5 K. The maximum injection time was 45 ms. The AGC target was 1e5. The HCD collision energy was 28%. MS was active from 8 to 120 min.

Proteomics data analysis

MS Raw data were processed by MaxQuant (Version 2.0.3.0). The peptide and protein identification were determined by the MaxQuant built-in Andromeda engine (Cox et al., 2011). that searches raw data against an Uniprot mouse proteome. False discovery rate threshold was set to 1%. The MaxLFQ algorithm (Cox et al., 2014) was used for label-free proteome quantification. The minimum ratio count for quantification was set to 1, while the final list of protein quantifications was filtered for proteins with a minimum of two peptides for each protein. The "Match Between Runs" feature was enabled. All statistics and bioinformatics were done by using Perseus (Version 1.6.15.0) (Tyanova et al., 2016). For the two-sample test, we performed a student t-test with a P value threshold of 5%. Missing values were replaced based on a normal distribution (width, 0.3; downshift, 1.8).

16S rDNA sequencing data analysis

16S rDNA sequencing raw data were processed with QIIME2. In brief, raw sequencing data were imported to QIIME2 and demultiplexed, then DADA2 was used for sequence quality control and feature table construction. The feature table was used for beta diversity analysis, taxonomic analysis, and differential abundance testing using QIIME2. Beta group significance was determined by permutational analysis of variance (PERMANOVA). Identification of taxa associated with different groups was determined using Analysis of Composition of Microbiomes (ANCOM).

Analysis of published single-cell data

For the violin plot gene expression profiles of scRNA-seq data of small intestinal epithelial cells (Haber et al., 2017), we plotted *Ramp1* expression using their analysis tool (https://singlecell.broadinstitute.org/single_cell/study/SCP44/small-intestinal-epithelium).

For the tSNE plot gene expression profiles of scRNA-seq data of purified goblet cells from small intestine and colon (Nyström et al., 2021), we plotted *Ramp1* expression with the authors' help.

CellPress

Supplemental figures

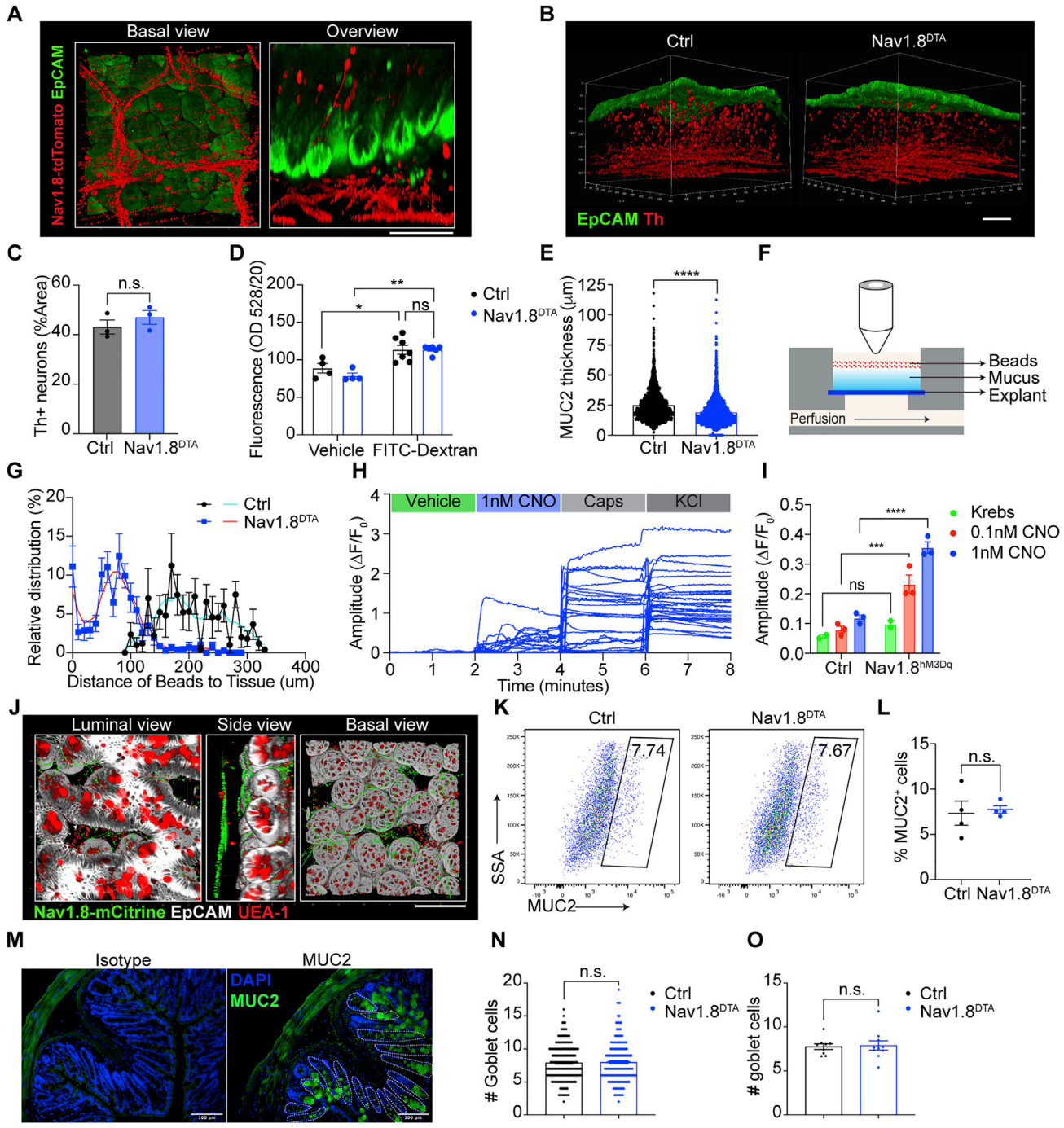

Figure S1. Nociceptors are juxtaposed with goblet cells and regulate colonic mucus production, related to Figure 1

(A) Whole-mount image of colonic tissue from Nav1.8^{tdTomato} mice stained for Nav1.8-tdTomato and EpCAM.

(B) Whole-mount image of colonic tissue from Nav1.8^{DTA} and control mice stained for EpCAM and tyrosine hydroxylase (Th).

(C) Quantification of Th^{+} neuronal innervation as %Th^{+} area in maximal projection images (MPI) shown in (B) (1 MPI per mouse; 3 mice/group).

(D) Fluorescence (OD 528/20) measurement of serum collected from Nav1.8^{DTA} and control mice orally gavaged with FITC-dextran or vehicle (n = 4–7 mice/group).

(legend continued on next page)

(E) Quantification of MUC2 thickness per measurement from Nav1.8^{DTA} and control mice (n = 20–30 measurements/mouse and 12–14 mice/group).
(F) Schematic of live colonic explant system for mucus thickness measurement.
(G) Pooled distribution (in black and blue) of fluorescent beads on colonic explants from Nav1.8^{DTA} and control mice (3–5 area/mouse; 3–4 mice/group). Smoothed curves (in cyan and red) were generated by averaging four neighbors of each distance.
(H and I) Traces (H) and quantification (I) of CNO (1 nM)- and vehicle (Krebs buffer)-induced calcium influx amplitude in KCl (40 mM)-responsive DRG neurons from Nav1.8^{hM3Dq} and control mice (n = 3/group).
(J) Whole-mount image of ileal tissue from Nav1.8^{hM3Dq} mice stained for Nav1.8-mCitrine, EpCAM, and UEA1.
(K and L) Flow cytometry plot (K) and quantification (L) of EpCAM^{+} epithelial cells showing the percentage of colonic MUC2^{+} goblet cells from Nav1.8^{DTA} and control mice (n = 4 mice/group).
(M) MUC2 and DAPI immunostaining for goblet cells in colon tissue from wild-type B6 mice.
(N and O) Quantification of colonic goblet cells per crypt (N) and per mouse (O) by MUC2 immunostaining from Nav1.8^{DTA} and control mice (n = 20–30 crypts/mouse and 8–10 mice/group).
Scale bars, 100 μm. One-way ANOVA in (D) and (I). Mann-Whitney test in (E) and (N). Student's test in (C), (L), and (O). Mean ± SEM. ns, not significant; *p < 0.05, **p < 0.01, ***p < 0.001, and ****p < 0.0001.

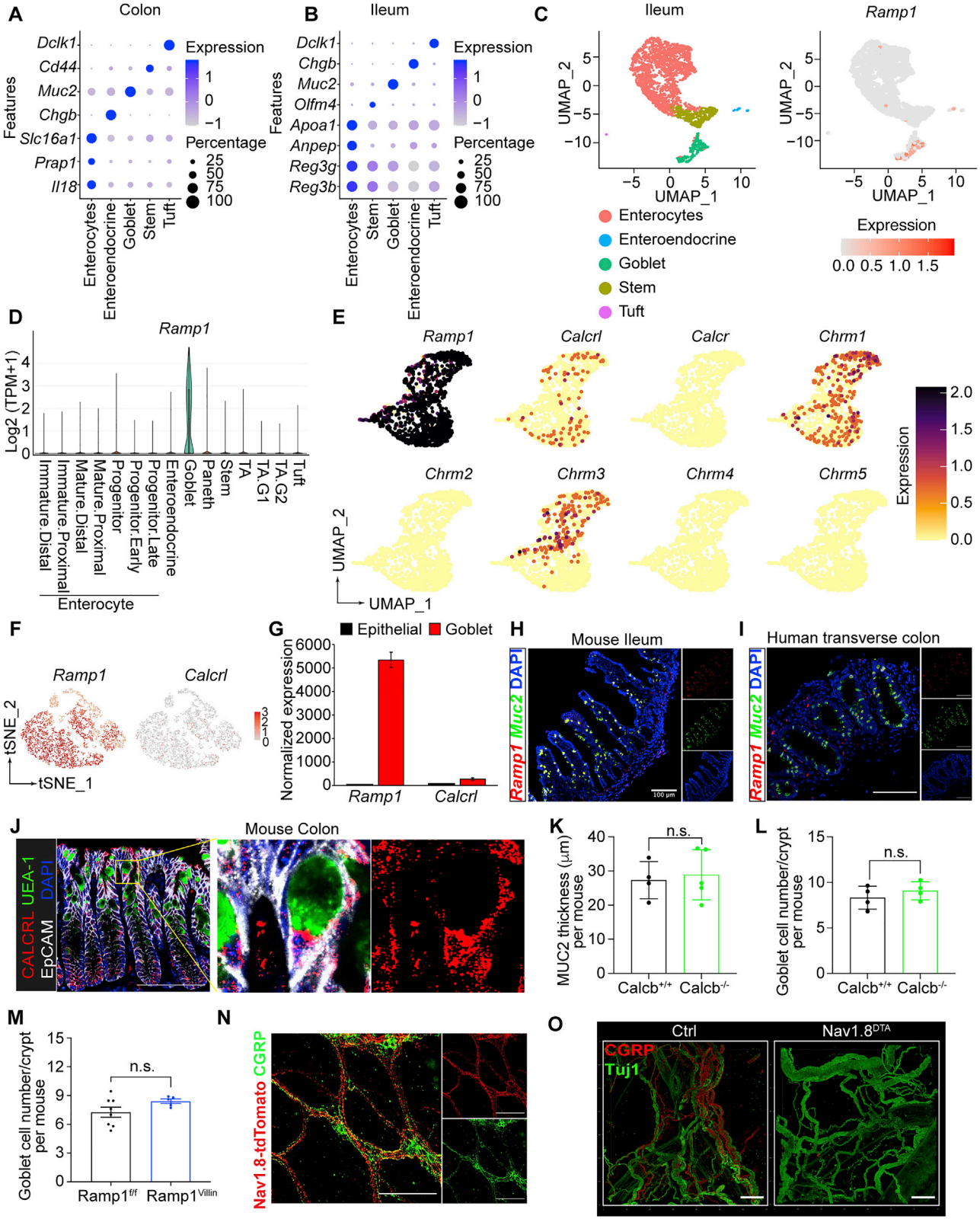

(legend on next page)

Figure S2. CGRP and epithelial Ramp1 maintain the intestinal mucus barrier, related to Figure 2

(A and B) Dot plot of average *Z*-scored expression (color) of marker genes (rows) in each inferred cell type in colonic (A) and ileal (B) epithelial cells from control *Nav1.8-Cre*$^{-}$*DTA*$^{fl/-}$ mice. (Dot size: percentage of cells in subset with positive expression of gene.)

(C) UMAP of scRNA-seq profiles of ileal epithelial cells from *Nav1.8-Cre*$^{-}$*DTA*$^{fl/-}$ mice, colored by inferred cell type (left) or *Ramp1* expression (right).

(D) Violin plot of *Ramp1* expression in ileal epithelial cell subsets, based on published scRNA-seq data (Haber et al., 2017).

(E) UMAP of scRNA-seq profiles of colonic goblet cells from *Nav1.8-Cre*$^{-}$*DTA*$^{fl/-}$ mice, colored by expression of the indicated receptors.

(F) t-distributed stochastic neighbor embedding (tSNE) plot of goblet cells (dots) sorted from the colon showing *Ramp1* expression (left) and *Calcrl* expression (right) (Nyström et al., 2021).

(G) Quantification of *Ramp1* and *Calcrl* expression in goblet cells (red) and non-goblet epithelial cells (black) sorted from colon (Nyström et al., 2021).

(H and I) *In situ* hybridization of *Ramp1* and *Muc2* in mouse ileum (H) and *RAMP1* and *MUC2* in human colon (transverse colon) (I).

(J) EpCAM, UEA1, and Calcrl staining of colon tissue from wild-type mice.

(K) Quantification of colonic MUC2 thickness per mouse from *Calcb*$^{+/+}$ and *Calcb*$^{-/-}$ mice (n = 4–5 mice/group).

(L) Colonic goblet cell number per crypt per mouse from *Calcb*$^{+/+}$ and *Calcb*$^{-/-}$ mice (n = 10–20 crypts/mouse and 4 mice/group).

(M) Colonic goblet cell number per crypt per mouse from Ramp1$^{fl/fl}$ and Ramp1^{Villin} mice (n = 10–20 crypts/mouse and 5–8 mice/group).

(N) Nav1.8-tdTomato and CGRP staining of colon tissue from Nav1.8^{tdTomato} mice.

(O) Tuj1 and CGRP staining of myenteric nerve preparations from Nav1.8^{DTA} and control mice.

Scale bars: 100 μm in (H)–(J), (N), and (O). Student's t test in (K)–(M). Mean ± SEM. ns, not significant.

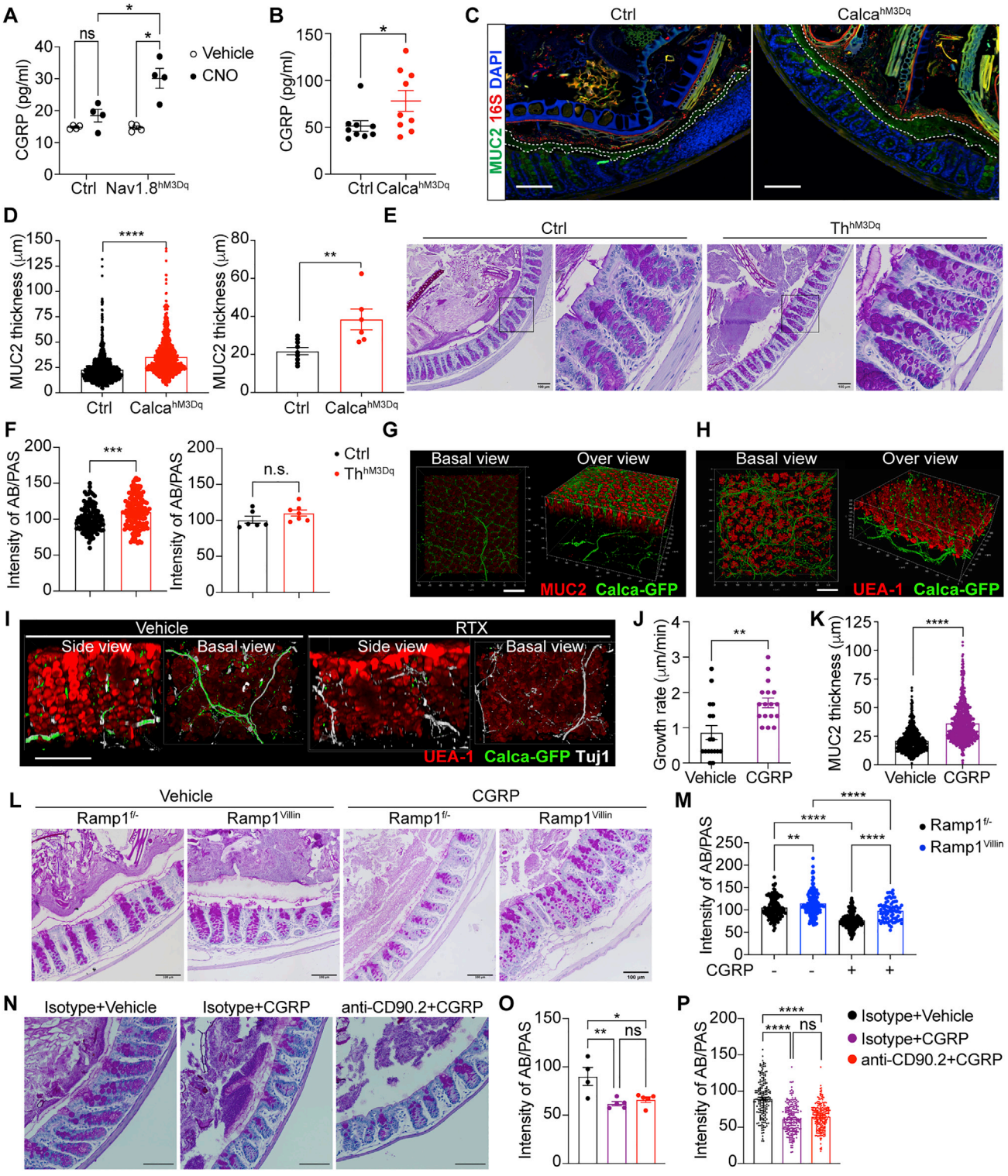

Figure S3. CGRP promotes mucus secretion in a Ramp1-dependent manner, related to Figure 4

(A) CGRP levels released by cultured Nav1.8^{hM3Dq} and control DRG neurons treated with CNO and vehicle (n = 4).

(B) CGRP levels in serum from Calca^{hM3Dq} and control mice treated with CNO (1 mg/kg) by i.p. injection for 10 min (n = 9 per group).

(C) MUC2, 16S rDNA, and DAPI staining of colon tissue from Calca^{hM3Dq} and control mice treated with CNO (1 mg/kg) i.p. for 10 min.

(D) Quantification of colonic MUC2 thickness per measurement (left) and per mouse (right) from mice in (C) (n = 20–30 measurement/mouse and 4–6 mice/group).

(legend continued on next page)

(E) AB/PAS staining of colon tissue from Th^{hM3Dq} and control mice treated with CNO (1 mg/kg) i.p. for 10 min.
(F) Quantification of colonic goblet cell mucus granule emptying by measurement of AB/PAS staining intensity per crypt (left) and per mouse (right) in mice from (E) (n = 20–30 crypts/mouse and 6–7 mice/ group).
(G and H) Whole-mount image of colonic tissue from Calca-GFP-DTR mice stained for CGRP-GFP and (G) MUC2 or (H) UEA1.
(I) Whole-mount image of colonic tissue from vehicle- or resiniferatoxin (RTX)-pretreated Calca-GFP-DTR mice stained for CGRP-GFP, Tuj1, and UEA1.
(J) Quantification of mucus growth rate per area from wild-type colonic explants treated with vehicle or CGRP (100 ng/mL) (n = 3–5 area/mouse and 4 mice/group).
(K) Quantification of colonic mucus thickness per measurement in wild-type B6 mice 10 min after CGRP (10 μg/mouse) i.p. injection (n = 20–30 measurements/ mouse and 7 mice/group).
(L) AB/PAS staining of colon tissue from $Ramp1^{Villin}$ and $Ramp1^{fl/fl}$ mice treated with either vehicle or CGRP (10 μg/mouse) by i.p. injection for 10 min.
(M) Quantification of colonic goblet cell mucus granule emptying by AB/PAS staining intensity per crypt in mice from (L) (n = 20–30 crypts/mouse and 3 mice/group).
(N) AB/PAS staining of colon tissues from isotype or anti-CD90.2 antibody pretreated wild-type mice followed by i.p. injection with vehicle or CGRP (10 μg/mouse) for 10 min.
(O and P) Quantification of colonic goblet cell mucus granule emptying by AB/PAS staining intensity per mouse (O) or per crypt (P) in mice from (N) (n = 20–30 crypts/mouse and 4–5 mice/group).
Scale bars: 100 μm in (C), (E), (G), (H), (I), (L), and (N). One-way ANOVA in (A), (M), (O), and (P). Mann-Whitney test in (D) (left panel), (F) (left panel), and (K). Student's test in (B) and (D) (right panel), (F) (right panel), and (J). Mean ± SEM. ns, not significant, *$p < 0.05$, **$p < 0.01$, ***$p < 0.001$, and ****$p < 0.0001$.

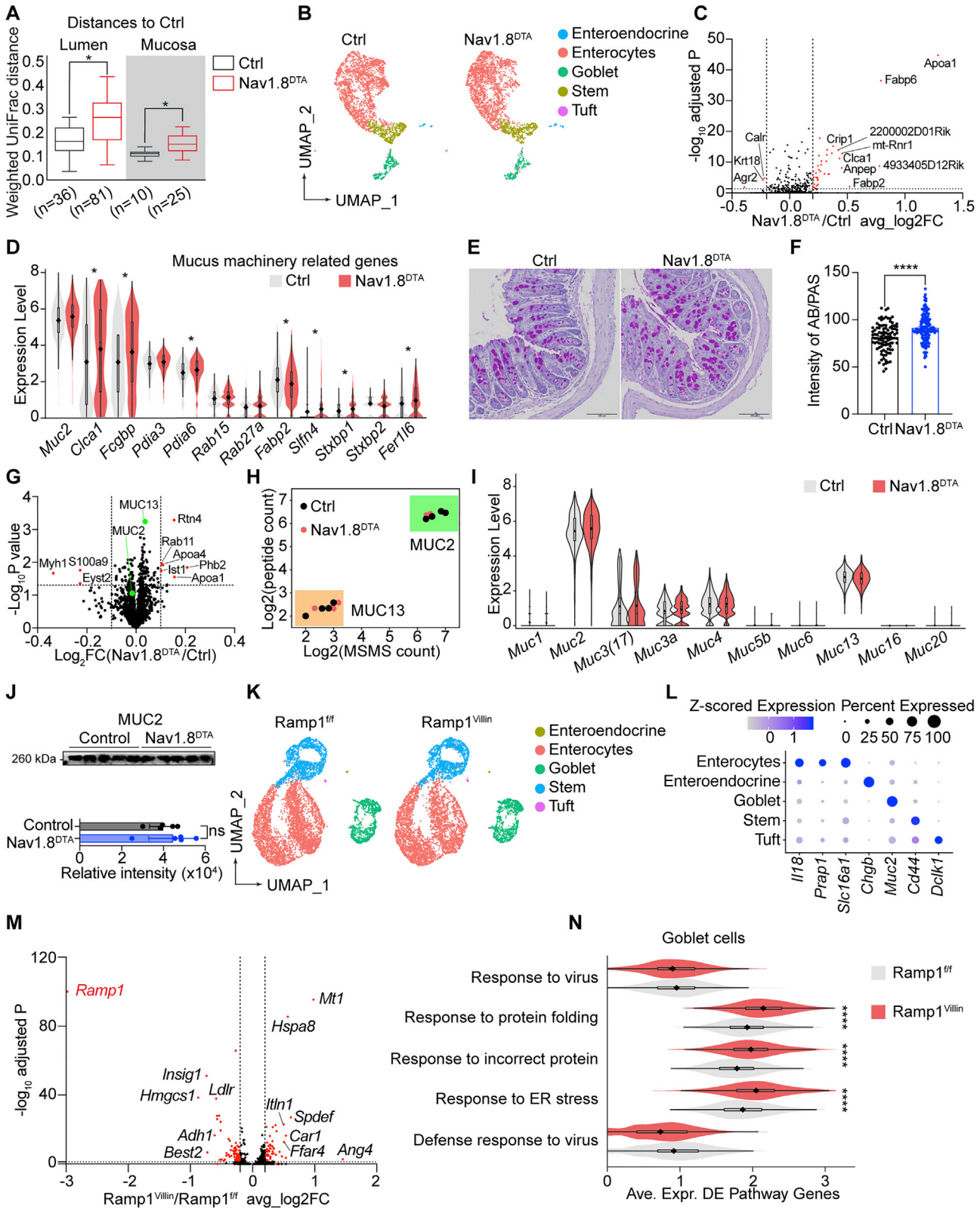

(legend on next page)

Figure S4. Both nociceptor ablation and epithelial Ramp1 deficiency induce increased gut epithelial stress and defense response, related to Figure 5

(A) Pairwise weighted UniFrac distance analysis of the composition of bacterial communities in colon lumen contents (lumen) and mucosal scrapings (mucosa) within the control group, and samples from Nav1.8^{DTA} mice compared with the control group (n = 5–9 mice/group, PERMANOVA, **q values < 0.005).

(B) UMAP plot of ileal epithelial cells, colored by inferred cell type, from Nav1.8^{DTA} and control mice.

(C) Volcano plot highlights 172 differentially expressed genes (red) in ileal goblet cells from Nav1.8^{DTA} versus control mice, based on thresholds (dotted lines) of |$\log_2$ fold change| > 0.2 and adj. p < 0.05.

(D) Violin plot of expression (y axis) of mucus machinery-related genes (x axis) in colonic goblet cells from Nav1.8^{DTA} and control mice.

(E) AB/PAS staining of colon tissues from Nav1.8^{DTA} and control mice.

(F) Quantification of colonic goblet cell mucus levels by measurement of AB/PAS staining intensity per crypt in mice from (E) (n = 20–30 crypts/mouse and 3 mice/group).

(G) Mass spectrometry analysis of colonic mucus samples from Nav1.8^{DTA} and control mice. 9 differentially expressed proteins (red) are identified (absolute value of $\log_2$ FC > 0.1 and adjusted p < 0.05). Mucin genes *Muc2* and *Muc13* are highlighted in green.

(H) Mass spectrometry quantification of MUC2 and MUC13 protein levels from colonic mucus layers from Nav1.8^{DTA} versus control mice (n = 4 mice/group).

(I) Violin plot of expression (y axis) of mucin genes (x axis) in colonic goblet cells from Nav1.8^{DTA} (red) and control (gray) mice.

(J) Western blot (top) and quantification (bottom) of MUC2 protein in colonic mucus layers from Nav1.8^{DTA} and control mice (n = 5 mice/group). Equal amount of total mucus protein from each sample was loaded.

(K) UMAP plot of colonic epithelial cells, colored by inferred cell type, from *Ramp1*^{Villin} and *Ramp1*$^{fl/fl}$ mice.

(L) Dot plot shows average *Z* scored expression (color) of marker genes (columns) in each cluster (rows) of colonic epithelial cells from Ramp1^{Villin} and Ramp1$^{fl/fl}$ mice.

(M) Volcano plot highlights 302 differentially expressed genes (DEGs, in red) in colonic goblet cells from Ramp1^{Villin} and Ramp1$^{fl/fl}$ mice, identified based on thresholds (dotted lines) of |$\log_2$ fold change| >0.2 and adjusted p < 0.05.

(N) Violin plot shows the distribution across colonic goblet cells of the average expression (x axis) of the DEGs, as in (M), that intersect with each of the indicated enriched pathways (y axis, GO biological processes), for Ramp1^{Villin} and Ramp1$^{fl/fl}$ mice.

Scale bars: 100 μm in (E). Mann-Whitney test in (D), (F), (I), and (N). Student's test in (J) (bottom). ns, not significant, *p < 0.05, ****p < 0.0001.

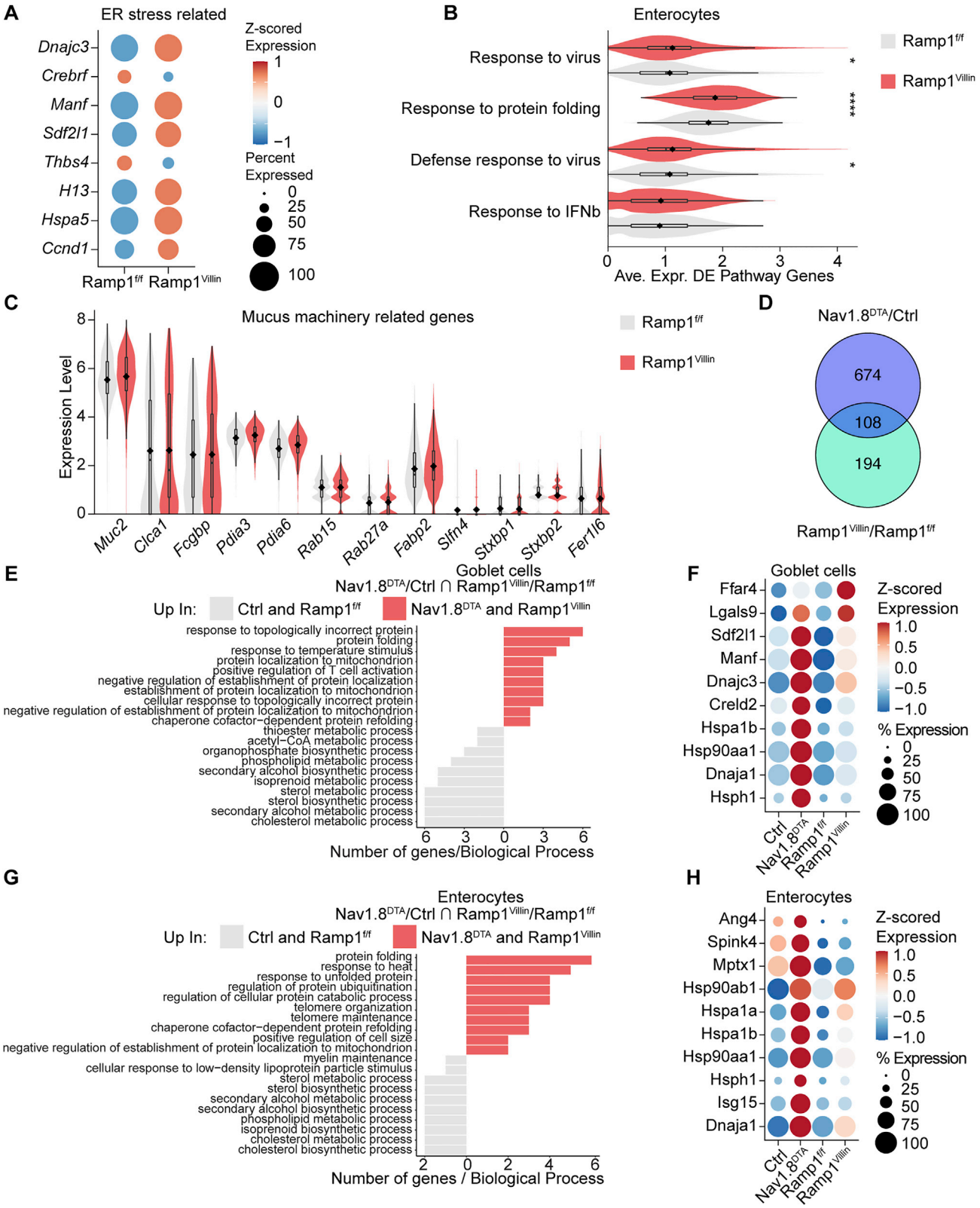

(legend on next page)

Figure S5. Common biological processes shared by nociceptor-deficient and Ramp1-deficient epithelial cells, related to Figure 5

(A) Dot plot showing average *Z*-scored expression of ER stress-related genes in goblet cells from Ramp1^{Villin} and Ramp1$^{fl/fl}$ mice.

(B) Violin plot, analogous to Figure S4N, for associated enriched pathways in enterocytes from Ramp1^{Villin} and Ramp1$^{fl/fl}$ mice.

(C) Violin plot of expression (y axis) of mucus-machinery-related genes (x axis) in colonic goblet cells from Ramp1^{Villin} and Ramp1$^{fl/fl}$ mice.

(D) Venn diagram showing overlap in DEGs in goblet cells from Nav1.8^{DTA} and Ramp1^{Villin} mice compared with their respective controls.

(E) GO biological processes enriched in the subsets of the 108 shared DEGs (as in D) that are up- or downregulated in goblet cells from Nav1.8^{DTA} and Ramp1^{Villin} compared with their controls.

(F) Dot plot showing average *Z*-scored expression (color) for genes that are differentially expressed in both Nav1.8^{DTA} and Ramp1^{Villin} goblet cells, compared with their controls.

(G) Analogous to (E), but for enterocytes from Nav1.8^{DTA} and Ramp1^{Villin} mice compared with control mice.

(H) Dot plot, analogous to (F), for enterocytes from Nav1.8^{DTA} and Ramp1^{Villin} mice compared with control mice.

Mann-Whitney test in (B) and (C). *$p < 0.05$, ****$p < 0.0001$.

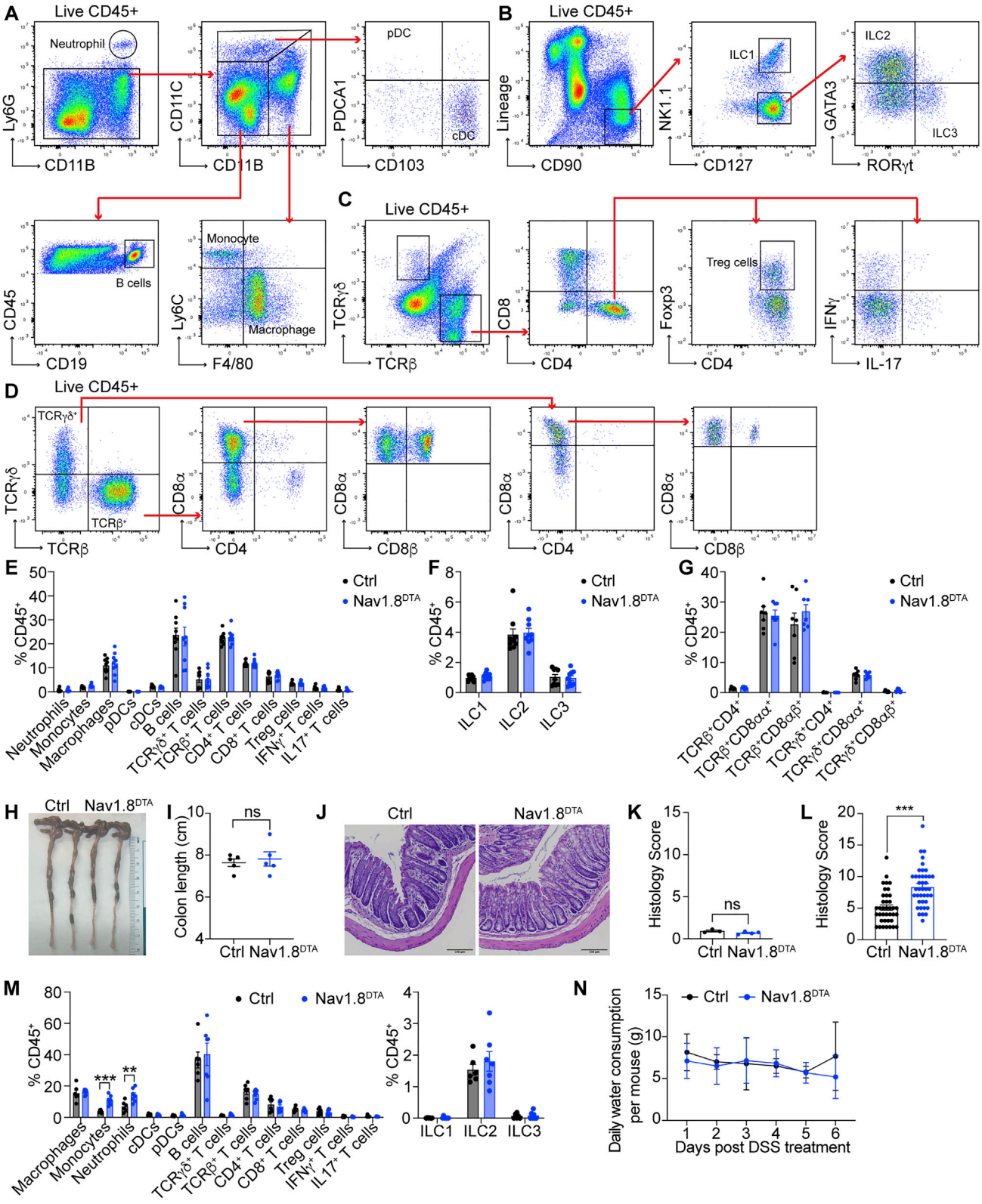

(legend on next page)

Figure S6. Immune profiling of nociceptor-ablated mice at baseline, related to Figure 6

(A–D) Flow cytometry gating of colonic lamina propria immune cells (A–C) and intraepithelial lymphocytes (D).

(E) Immune profiling (% of $CD45^+$ cells) of colonic lamina propria cells from $Nav1.8^{DTA}$ and control mice (n = 9 mice/group).

(F) Immune profiling (% of $CD45^+$ cells) of colonic lamina propria ILCs from $Nav1.8^{DTA}$ and control mice (n = 9 mice/group).

(G) Immune profiling (% of $CD45^+$ cells) of colonic intraepithelial lymphocytes from $Nav1.8^{DTA}$ and control mice (n = 7 mice/group).

(H) Image of colons from $Nav1.8^{DTA}$ and control mice at baseline.

(I) Colon length measurement of $Nav1.8^{DTA}$ and control mice at baseline (n = 5 mice/group).

(J) H&E staining images of colons from $Nav1.8^{DTA}$ and control mice at baseline.

(K) Histology scoring per mouse of colon tissues from $Nav1.8^{DTA}$ and control mice at baseline (n = 5 mice/group).

(L) Histology scoring per area of colon tissues from $Nav1.8^{DTA}$ and control mice 10 days after DSS treatment as in Figure 6B (n = 4 areas/mouse and 4 mice/group).

(M) Immune profiling of colonic lamina propria from mice (as in Figure 6H) on day 10 post DSS treatment (n = 6–7 mice/group) shown as $\%CD45^+$ cells. Left panel shows myeloid and adaptive cell populations. Right panel shows ILCs.

(N) Daily water consumption per mouse of $Nav1.8^{DTA}$ and control mice during 3.5% DSS treatment (n = 7–9 mice/group).

Scale bars: 100 μm in (J). Multiple t test in (E)–(G), (M), and (N). Mann-Whitney test in (L). Student's t test in (I) and (K). Mean ± SEM. ns, not significant, $^{**}p < 0.01$, $^{***}p < 0.001$.

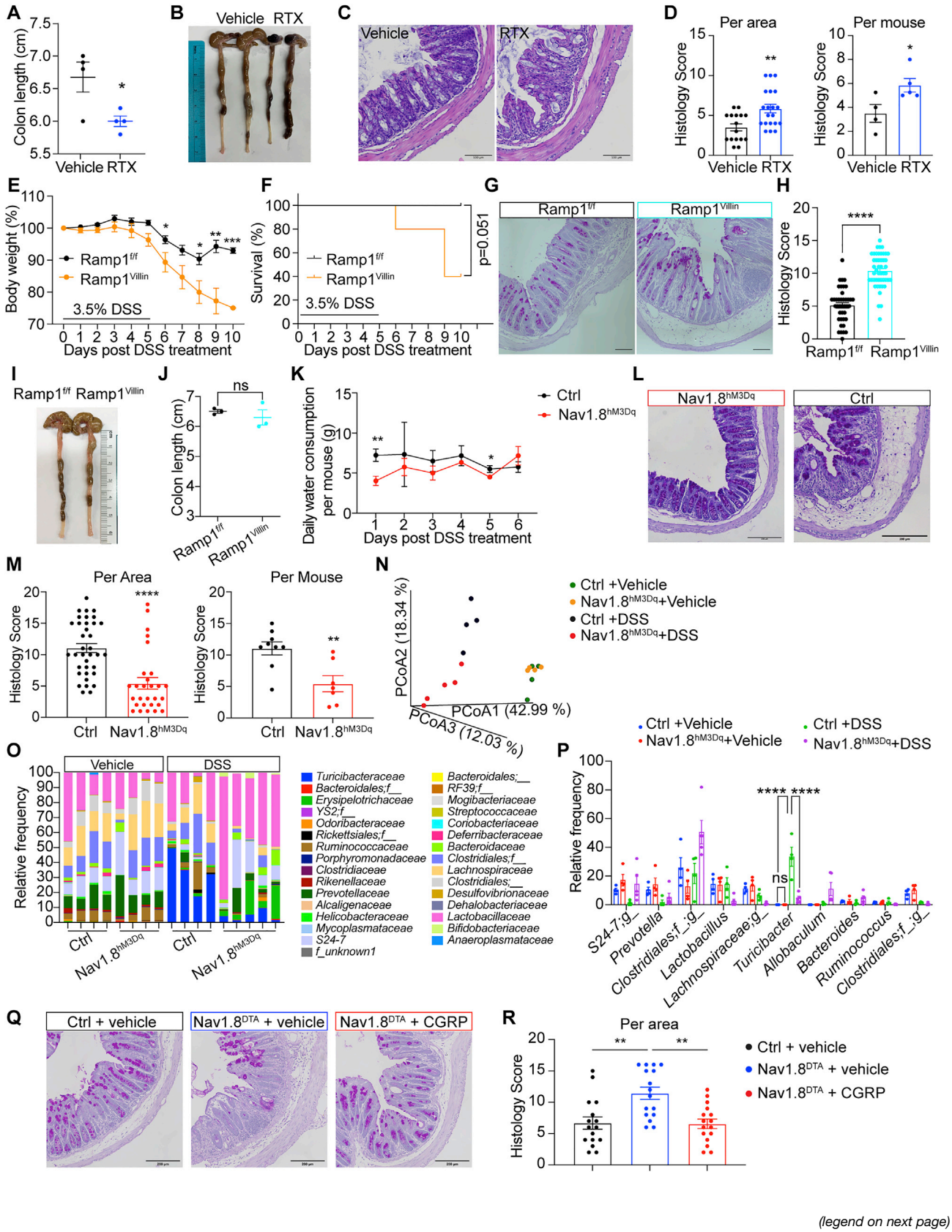

(legend on next page)

Figure S7. Nociceptors and epithelial Ramp1 mediate host protection against intestinal colitis, related to Figures 6 and 7

(A) Colon length of RTX- and vehicle-pretreated mice treated with 2.5% DSS for 5 days (n = 4 mice/group). Measurement on day 8 post DSS treatment.
(B) Image of colons from mice in (A).
(C) H&E staining images of colons from mice in (A).
(D) Histology scoring per area (left) and per mouse (right) of colon tissues from mice in (A) (n = 4 areas/mouse and 4–5 mice/group).
(E) Body weight of Ramp1^{Villin} and Ramp1$^{fl/fl}$ mice treated with 3.5% DSS in drinking water for 5 days (n = 5 mice/group).
(F) % Survival of Ramp1^{Villin} and Ramp1$^{fl/fl}$ mice treated with 3.5% DSS in drinking water for 5 days (n = 5 mice/group).
(G) AB/PAS staining images of colons from Ramp1^{Villin} and control mice 8 days post 2.5% DSS treatment.
(H) Histology scoring per area of colon tissues from Ramp1^{Villin} and control mice 8 days post 2.5% DSS treatment from Figure 6K. (n = 4 areas/mouse and 4 mice/group).
(I) Representative image of colons from Ramp1^{Villin} and control mice at baseline.
(J) Colon length of Ramp1^{Villin} and control mice at baseline (n = 3 mice/group).
(K) Daily water consumption per mouse in Nav1.8^{hm3Dq} and control mice during 3.5% DSS treatment (n = 6 mice/group).
(L) AB/PAS staining images of colons from Nav1.8^{hm3Dq} and control mice 8 days post 3.5% DSS treatment.
(M) Histology scoring per area (left) and per mouse (right) of colon tissues from mice in (K) (n = 4 areas/mouse and 6–9 mice/group).
(N) Principal coordinates analysis (PCoA) of weighted UniFrac distance measurements of colonic luminal microbiomes from Nav1.8^{hM3Dq} and control mice 8 days after treatment with DSS (3.5%) plus CNO (0.5 μg/mL) or vehicle (n = 4–5 mice/group).
(O and P) Nav1.8^{hM3Dq} and control mice were treated or untreated with DSS (3.5%) plus CNO (0.5 μg/mL) in drinking water for 6 days and colon luminal contents were collected on day 8 for 16S rDNA sequencing analysis at the family level (E) and the genus level (F) (n = 4–5 mice/group).
(Q) AB/PAS staining images of colons from Nav1.8^{DTA} and control mice treated with CGRP (10 μg/day) or vehicle during DSS colitis. Images from 8 days post 3.5% DSS treatment.
(R) Histology scoring per area of colon tissues from Nav1.8^{DTA} and control mice treated with CGRP (10 μg/day) or vehicle on day 8 post DSS treatment. (n = 4 areas mouse and 4 mice/group).
Scale bars: 100 μm in (C) and (G); 200 μm in (L) and (Q). Student's t test in (A) and (D) (right panel), (J), and (M) (right panel). Mann-Whitney test in (D) (left panel), (H), and (M) (left panel). Multiple t test in (E) and (K). Log-rank test in (F). Two-way ANOVA in (P). One-way ANOVA in (R). Mean ± SEM. ns, not significant, *$p < 0.05$, **$p < 0.01$, ***$p < 0.001$, and ****$p < 0.0001$.